

Understanding and modelling wear rates and mechanisms in fretting via the concept of rate-determining processes - contact oxygenation, debris formation and debris ejection

P.H. Shipway, A.M. Kirk, C.J. Bennett, T. Zhu

Faculty of Engineering, University of Nottingham, UK

Keywords: modeling, RDP, tribologically transformed structures (TTS), third body approach

1 Abstract

A new framework which describes the role of three key processes in fretting wear of metals is proposed, with these three processes being: (i) oxygen transport into the contact; (ii) formation of oxide-based wear debris in the contact and (iii) ejection of the wear debris from the contact. Based upon a physical understanding, rates of the three key processes are proposed, which provide a basis for the influence of test parameters (such as contact geometry, applied load, slip amplitude, fretting frequency etc) on the three rates to be understood. To maintain system equilibrium in steady-state fretting, the three processes must operate at the same rate as each other (debris cannot be ejected from the contact faster than it is formed, and debris cannot be formed faster than it is ejected). Accordingly, the *observed wear rate* is the rate of the process with the lowest rate of the three processes, with this process being termed the *rate-determining process*. The effect of test parameters on the three key processes differs, and thus the effect of changes in any test parameter on the observed rate of wear will itself be dependent upon which of the three processes is rate-determining.

A number of assumptions have been made in deriving the equations which describe the key processes and it is recognised that these equations themselves may be refined in light of future research; however, any such revised equations can simply replace those proposed as part of the rate-determining process framework.

The framework can be applied to both conforming and non-conforming contact geometries. In tests with non-conforming contact geometries, the contact size increases with wear; since it is proposed that the rates of two of the three processes (oxygen transport and debris ejection) are dependent upon the size of the contact, the rate determining process can change during a test and the rate of wear will continually fall when either of these processes are rate-determining. This complexity means that the evolution of the wear volume can only be evaluated numerically through the use of a time-marching analysis in such cases. In contrast, in tests with conforming contact geometries, the contact size does not change as wear occurs, and so there will be no changes in the rate-determining process as wear proceeds.

It is recognised that this framework addresses wear under steady-state conditions and does not consider the initial period of exposure where steady-state conditions are being developed. In the case of conforming contacts where the contact size is large, the duration of the initial transient period may be substantial and may form a significant proportion of the test duration or component lifetime. This needs to be recognised both in the design of tests and in the application of this framework.

2 Introduction

Fretting wear is a form of degradation that is commonly observed in a wide range of engineering applications due to system vibrations giving rise to relative motion between contacting surfaces. Fretting wear typically occurs at an interface in which oscillating tangential loads result in slip occurring across the interface; in fretting, the amplitude of slip displacement (typically of the order of tens of micrometres) is small relative to the size of the contact. As such, a region of the interface therefore remains covered (occluded) from the atmosphere throughout the wear process.

Fretting of metals is characterised by the formation of oxide-based debris in the fretting contact and its expulsion from that contact. The small displacement amplitudes that characterise fretting wear hence result in the following two key processes potentially having their rates limited:

- (i) transport into the contact of active species (typically oxygen) from the surrounding environment;
- (ii) transport out of the contact of wear products (typically oxide-based wear debris).

The retention of wear debris in a contact undergoing fretting wear plays a critical role in determining the operative wear mechanism and the extent of material removal, highlighted by the “third body approach” to tribology outlined by Godet and co-workers [1–5] in the 1980s and developed throughout the following decades. In this approach, it was argued that in fretting the traditional definition of wear as the removal of material from surfaces is not sufficient to describe the amount of material lost due to wear; instead, a definition of wear needs to account for the flows of debris out of the contact and should instead be defined as the amount of material ejected from the contact.

A widely used approach for the prediction of wear rates in fretting is that outlined by Archard [6]; this was originally derived for sliding wear, a mode of wear in which both transport of species into the contact and transport of species out of the contact occur readily and hence play a diminished role when compared to their role in fretting. Consequently, it has been argued that the Archard wear equation (and the energy wear approach derived from it [7]) is suited only to the prediction of the rate of *formation* of debris particles, but cannot account for the rate of transport of species (as outlined previously) into and out of a fretting contact [8]. Moreover, it has been further argued that the rate of transport of species into and out of the contact may indeed act to limit the rate of formation of debris particles (implying that the Archard approach is not sufficient in this respect). In summary, it is proposed that in order for

new wear debris to form, wear debris previously produced and present in the contact must be ejected from the contact to allow the wear process to continue. Debris cannot be ejected from the contact faster than it is formed, and to maintain equilibrium, debris cannot be formed faster than it is ejected. It is proposed that the observed rate of wear will be determined by the process with the smallest rate, with this process being termed the *rate-determining process* (RDP) [9–11].

The value of the RDP approach was demonstrated by Zhu et al. [9]. In this work, the role of transport of species (such as oxygen) into the contact was not considered, and therefore the overall wear rate was assumed to be controlled by the slowest of two critical processes, namely:

- (i) the creation of debris from the contacting surfaces (debris formation);
- (ii) the flow of debris out of the contact (debris ejection).

It was postulated that the ejection of debris from the contact is dependent upon the physical size of the contact as illustrated in Figure 1; the observed wear rate for a given contact (wear scar) size is the smaller of the two rates (i.e. the lower of the two lines). This is relevant both for conforming contact geometries (such as flat-on-flat) where the scar size is independent of the amount of wear and for non-conforming geometries (such as sphere-on-flat, cylinder-on-flat and crossed-cylinders) where the wear scar increases in size as wear takes place. Referring to Figure 1, it is noted that in the case of non-conforming contact geometries, the RDP may change during the course of a test as the scar increases in size; moreover when debris ejection is the RDP in such a situation, the rate will continually fall as the scar increases in size (i.e. as the test proceeds).

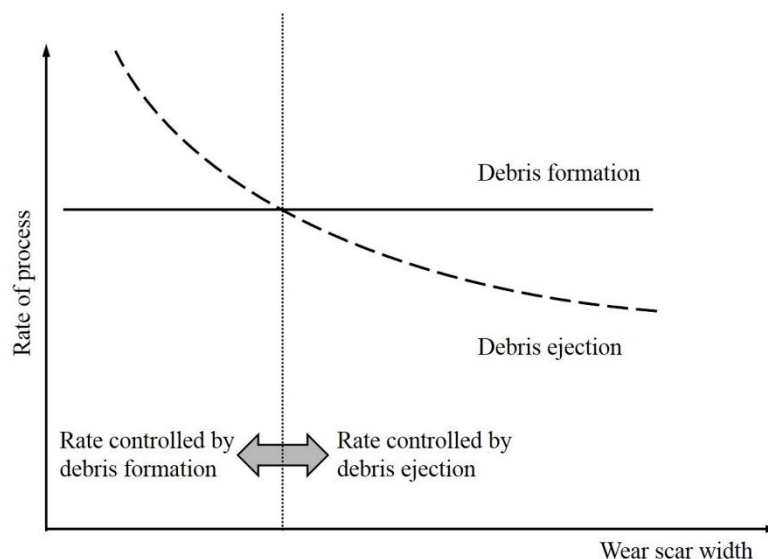


Figure 1 Schematic diagram illustrating the proposed dependence of wear rate upon the relative rates of debris formation and ejection with increasing wear scar width presented by Zhu et al. [9]; it was proposed that wear rate is controlled by whichever of the two processes is rate-determining (i.e. the lower of the two lines) at a given scar width.

This has significant implications for our understanding of fretting. In developing an understanding of the effects of various parameters on fretting wear (either in experimental testing or in service), there is a fundamental need to determine whether the observed rate of wear is controlled by the rate of debris formation or the rate of debris ejection. Moreover, in both engineering service applications and in experimental research, fretting often involves non-conforming contact configurations (i.e. contacts for which the contact size increases as wear proceeds); in this situation, both the RDP and the rate of wear may change as wear proceeds and this must be taken into account if the evolution of wear is to be predicted accurately. Recently, Zhu and Shipway [8] demonstrated that for commonly-employed non-conforming experimental configurations (cylinder-on-flat, sphere-on-flat and crossed cylinders) in situations where debris ejection from the contact remains the RDP throughout its duration, then the wear equation can be written:

$$V = KR^{n-1} E^n$$

where V is the wear scar volume, R is the radius of the non-plane specimen(s) in the pair, E is the frictional energy dissipated, and n is a constant which varies between 0.67 and 0.8 depending upon the geometry and assumptions made regarding the governing equation.

Debris flow from the contact can be significantly influenced by the tendency to sinter under certain conditions. It is well known that in fretting at elevated temperatures, stable, coherent layers of sintered wear debris have been observed in numerous experimental investigations, with these being termed “glaze layers” due to their smooth, glassy appearance [12–18]. The formation of glaze layers has been reported to be dependent on a number of factors, including displacement amplitude [13], fretting frequency [19] and relative proportions of alloying elements [20], but above all to be highly dependent on the environmental temperature [12,14,19,21,22], with glaze layers only being observed to form at elevated temperatures. The formation of a glaze layer is typically associated with a significant reduction in wear rate such that wear almost entirely ceases, and it is argued that this change in wear regime points to the need to consider the sintering of debris in predictive modelling of wear rates.

We will now turn our attention to the issue of the requirement for oxygen transport into the contact to form oxide-based debris. Oxygen will be consumed in the formation of such debris, and it was first suggested by Mary et al. [23,24] that under certain fretting conditions, the rate of oxygen transport into the interface is not sufficient to replenish oxygen consumed in the fretting process. Iwabuchi et al. [25,26] conducted fretting tests in environments with varying oxygen concentrations and observed that oxygen pressure significantly influenced the mechanism of fretting in steel pairs, noting a critical pressure below which a transition in wear mechanism occurs from an oxidative-abrasive mechanism to an adhesive mechanism. In the adhesive mechanism, lower wear rates were observed; metallic debris was formed but this was mostly retained in the contact as it transferred between the opposing surfaces (as opposed to being expelled from it). Similarly, Fouvry et al. [27] observed that the wear rate in adhesive (oxygen-starved) contacts was less than a third of that observed in abrasive (oxygen-rich) contacts. In work examining the fretting of a high strength steel pair over a range of displacement amplitudes and frequencies, Kirk et al. [11] observed that the wear debris

ejected from the contact consisted almost entirely of metal oxides (> 94 wt% oxide in all cases) even under conditions when the formation of a substantial sub-surface tribologically transformed structure in the wear scar indicated significant first-body (metal-metal) contact.

In drawing this link between the insufficiency of the rate of oxygen transport into the contact and the adhesive mechanism of wear, it is noted that adhesive wear is sometimes observed at the early stages of fretting of a contact between metallic bodies which then develops into an oxidative-abrasive mechanism as the test proceeds [8]. Initially, there is no oxide debris layer separating the two surfaces, and adhesion may be observed (depending upon the conditions and the duration of the test) along with transient behaviour in the evolution of the coefficient of friction [28–31]. This type of adhesive wear is termed the initial-transient adhesion, and is not necessarily associated with an insufficiency of oxygen being transported into the contact. This initial-transient adhesion is not the subject of this paper with the adhesive wear addressed here being that which takes place in the steady state where oxygen transport into the contact is insufficient to form debris at a rate necessary to separate the metallic bodies making up the contact.

In light of these observations, it has been proposed [11] that if oxide is unable to form then wear (i.e. material ejection from the contact) does not occur and that any metallic debris formed is retained within the contact rather than ejected from it. It was argued that it follows that transport of oxygen into the contact is therefore a necessary condition for wear to proceed. As such, it was proposed that there is another potential RDP in the process of fretting, namely that of oxygen transport into the contact.

This proposal is in accord with a wide body of literature where the effects of the rate of oxygen transport into fretting contacts have been addressed [23–26,32]. Work by Van Peteghem et al. [33] and Warmuth et al. [34] examined the effect of frequency on fretting, indicating that higher frequencies resulted in less time for oxygen transport into the contact and thus to an insufficiency of oxygen to form oxide-based debris at the required rate, with this being associated with oxygen transport being the RDP when certain conditions are satisfied [10]. Fouvry et al. [27] developed a “contact oxygenation description of fretting”, which provided a framework for interpreting the effects of fretting parameters on wear rates and mechanisms in terms of their effect on oxygen concentration in the contact. In this, the contact zone was divided into a region dominated by adhesive wear (where the oxygen concentration was below a particular threshold value) and a region dominated by abrasive wear (where the oxygen concentration was above that critical value) [35]. It was suggested that this threshold partial pressure of oxygen is very low, being in the range of 0.1 Pa [36].

This concept has since been developed by Baydoun and co-workers [35–38] who presented a model for the flow of oxygen into fretting contacts, using this to predict the concentration of oxygen across the wear scar and hence determine whether oxygen-starved “adhesive zones” develop under a given set of conditions, and (if so) the size of such zones. This is a significant step towards quantitative modelling of oxygen transport in fretting contacts, although it has not yet been applied to modelling the associated impact of restricted oxygen transport on wear rates.

A critical element in the development of these models is that oxygen is consumed in the formation of wear debris [23,24]. In the recent advection-dispersion-reaction (ADR) model [36], it was assumed that the consumption (reaction) rate of oxygen in the contact is proportional to its concentration. Moreover, on the basis of experimental data, it was assumed that the oxygen consumption rate in the contact is also proportional to ω^γ , where ω is the frictional power per unit area dissipated in the contact and γ is a constant which was evaluated to be 0.47. Whilst these assumptions allowed the construction of a model which is able to quantitatively rationalise the effects of various test parameters the distribution of adhesive and abrasive zones in a fretting scar, the physical basis upon which these assumptions are made is not clear. Moreover, whilst this model is predictive in terms of the wear mechanisms operative in a fretting contact (and their spatial distribution), the challenge of incorporating the concept of contact oxygenation into a predictive model for the rate of wear still remains.

In the present work, a novel formulation is outlined for prediction of wear rates and mechanisms in fretting based on the concept of the rate-determining process (RDP) which incorporates both the role of oxygen transport into the contact to form oxide-based debris and the role of expulsion of that debris from the contact.

Only fretting behaviour at ambient temperature is considered, and as such the effect of temperature in the formation and retention of debris (including whether a glaze forms and effectively halts the progress of wear) is not addressed; it is argued that this does not significantly impact the validity of the model over the range of conditions examined, although this is a necessary consideration if fretting behaviour at higher temperatures is to be addressed. Although the concepts outlined have general applicability to fretting wear of contacts with both conforming and non-conforming geometries, it is recognised that there is added complexity with non-conforming contact geometries given that there may be a change in both the RDP and the rate of wear as the contact wears (due to the increase in contact size with wear in such cases). In particular, the potential for change from one RDP to another during the course of a test as the scar size increases means that attempts to develop an all-encompassing wear equation for such situations is futile. Instead, for non-conforming contacts, a time-marching approach is employed which is able to account for changes in the RDP as a result of the evolving contact size. The outputs from the model are compared to experimental data which have been previously reported in the literature.

3 The basis for a new model for fretting wear

In this paper, the focus will be upon on the more complex situation of fretting wear of a non-conforming contact geometry (where the scar size changes as wear proceeds); however, the work has equal validity for the simpler situation of a confirming contact. A framework for a model will be presented which allows the effects of various parameters on the observed rate of wear to be considered. The model assumes that the process of wear itself (i.e. continual material removal from the contacting surface and its expulsion from the contact in the form of debris) involves the chemical reaction of a metallic surface material to form oxide debris (the model as outlined would require appropriate modification to be applied in other situations). Likewise, the model is developed in detail for just one of the commonly employed non-

conforming contact geometries commonly utilised in laboratory fretting research, namely the cylinder-on-flat geometry; again, whilst the concepts presented are general, the details of the model presented would require modification to allow application to other non-conforming pairs with different geometries. Moreover, as previously stated, the general approach is equally relevant to fretting of conforming pairs, but the complexities of changes between RDPs and changes in the rates of wear as the test proceeds do not need to be considered in such cases. The framework only considers fretting under steady-state conditions, and does not address the initial transient period where there can also be changes in wear and damage mechanisms. These transient periods are often very brief and (depending upon the length of the total exposure) can reasonably be ignored; however, in fretting with larger contact sizes (as often deployed in tests with conforming contacts or in service environments), this initial transient period can be very long. Accordingly, care must be taken to ensure that this framework is applied (as designed) only to situations running under steady-state conditions, and that tests are run for durations long enough to ensure that the initial transient can safely be ignored. In developing the model, reference is made to a recent paper [36] where the fretting of steel against steel in a cylinder-on-flat geometrical arrangement as illustrated in Figure 2 was addressed. It was shown that the total wear volume, V (i.e. the sum of the worn volume of the two individual specimens) is very well described by the volume of intersection of the plane and cylinder (see Figure 3); as such, the wear scar width and the wear scar volume could be related to each other by the following simple geometrical relationship (based upon the area of a circular segment):

$$V = L \left(R^2 \arcsin \left(\frac{b}{R} \right) - b \sqrt{R^2 - b^2} \right) \quad \text{Equation 1}$$

Here, L is the line length of the contact, R is the radius of the cylindrical specimen and b is the contact semi-width (i.e. the half-length of the chord). Moreover, this relationship was shown to hold over a wide range of scar widths and volumes (see Figure 4).

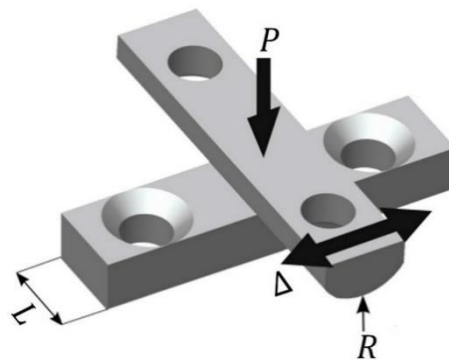


Figure 2 Schematic diagram of cylinder-on-flat specimen configuration used in fretting tests; $L = 10$ mm, $R = 6$ mm.

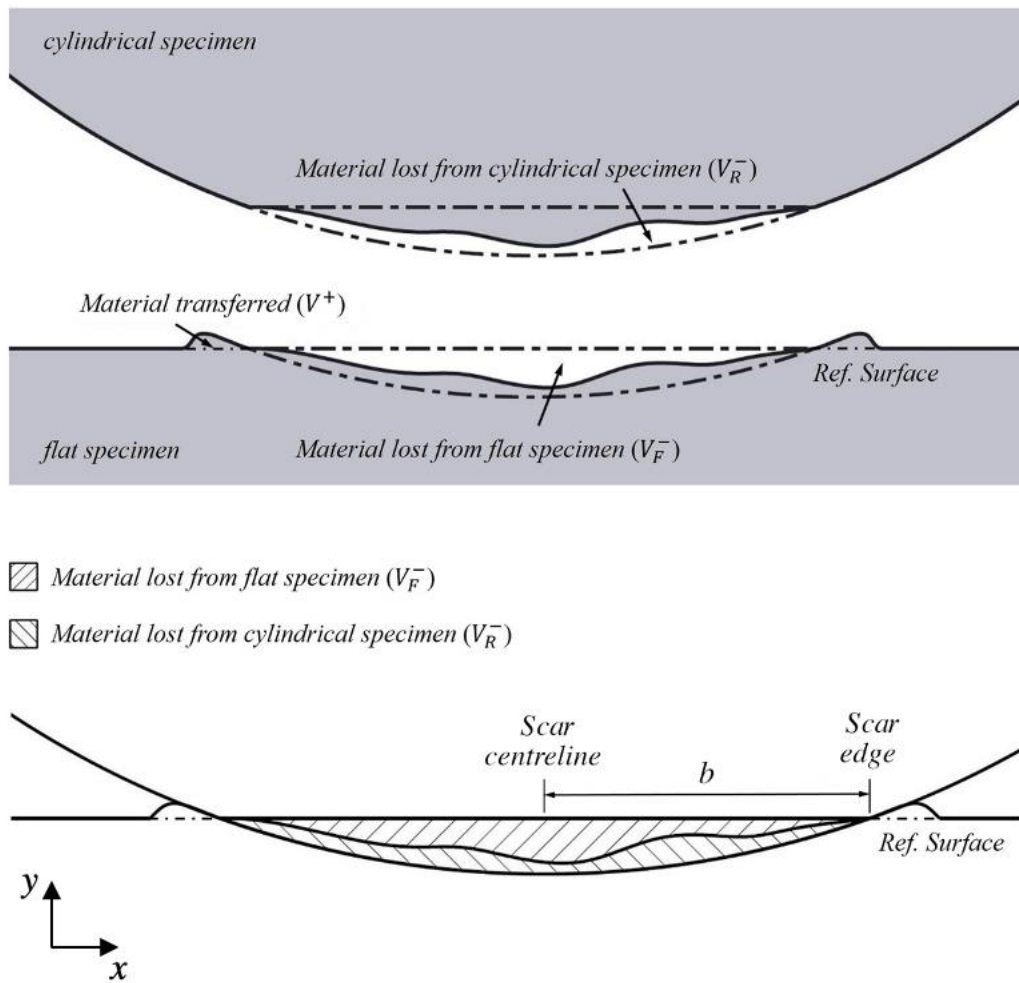


Figure 3 Schematic diagram illustrating material removal between the two specimens of the pair where the combined wear on the two specimens results in a total worn volume equivalent to the minor cylindrical segment of intersection. After [9].

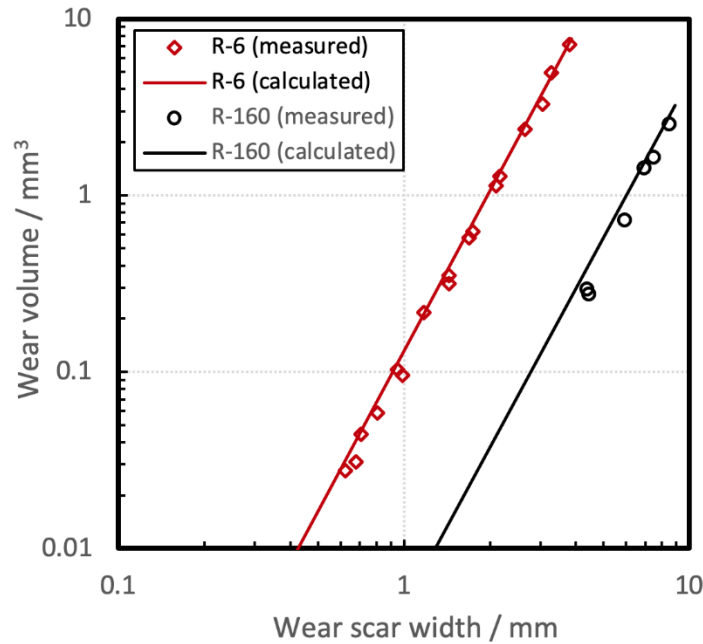


Figure 4 Measured total wear scar volumes for a fretting pair plotted against the scar width, $2b$, for a cylinder-on-flat fretting pair with cylinders of two radii ($R = 6$ mm and $R = 160$ mm). Alongside the measured values are the predicted relationships based upon Equation 1. After [9].

To preserve this geometrical relationship, it is argued that the instantaneous rate of surface recession (wear), summed over the two specimens in the pair, must be the same at all positions within the wear scar (although it can vary temporally). This apparently simple statement is a foundational concept within this work. It is noted that this is in contrast to the work of Fouvry and co-workers [27,36] where it is inferred that different wear rates exist in different parts of a fretting contact.

3.1 The rate-determining process

The development of the model here is built upon three key physical processes which govern the overall process of wear, which can be summarised as follows:

1. Relative motion at the contacting surfaces results in wear; the rate of removal of material from the surface to form oxide wear debris is described by the Archard wear rate.
2. Oxygen is transported into the contact to allow oxide wear debris to be formed; furthermore, it has been proposed that oxygen transport into fretting contacts is mainly driven by diffusion [38]. If oxygen transport is the RDP, then the rate of formation of oxide wear debris is proportional to the rate of oxygen transport.
3. The oxide debris formed is transported out of the contact with this being required for wear of the two first bodies to continue. This prevents the debris layer from growing in thickness to a point where the relative displacement of the two first bodies can be accommodated by strains within the debris bed itself; if this were to occur, there would

be no relative motion at the surfaces of the first-bodies and thus wear by abrasion or adhesion would cease.

In the steady-state, the process of wear involves these three processes (oxygen transport into the contact, Archard wear and debris ejection from the contact) working at the same rate (debris cannot be ejected from the contact faster than it is formed, and to maintain equilibrium, debris cannot be formed faster than it is ejected). Moreover, it is proposed that the observed rate of wear will be the *smallest* of the three rates described, with that process being described as the rate-determining process (RDP).

Later in this paper, it will be argued that the rates controlled by oxygen ingress and debris ejection from a fretting contact (either conforming or non-conforming) are dependent upon the contact width as illustrated schematically in Figure 5; in a figure such as this, the RDP is identified as the process with the smallest rate, and in this illustration, the RDP changes with increasing contact width from an Archard-controlled wear rate to a debris-ejection controlled wear rate and then to an oxygen-transport controlled wear rate.

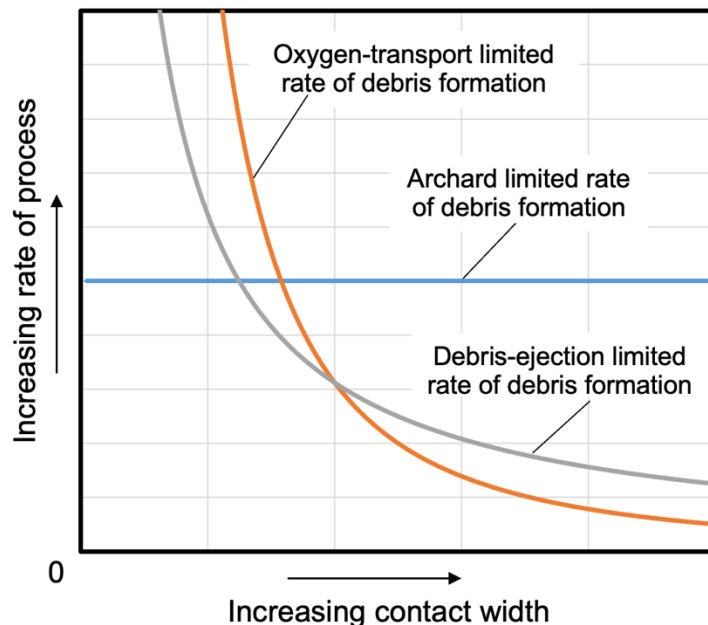


Figure 5 Schematic diagram illustrating the variations in the three rates as a function of contact width. The operative process at any contact width is that with the lowest of the three rates, with the observed rate being the rate of the operative process (RDP). Whilst this relates to both conforming and non-conforming contacts, it is noted that in the case of non-conforming contacts, the contact width increases as wear proceeds and accordingly there may be changes in the RDP throughout the exposure.

In the case of fretting with a non-conforming contact geometry, the size of the wear scar will increase as wear proceeds, and therefore with the increase in energy dissipated in the contact. An example of such a situation where there are two changes in the RDP as the energy dissipated increases is shown in Figure 6a. In Regime I, the RDP is the Archard-limited rate of debris formation; in Regime II, the RDP is the debris-ejection limited rate of debris formation and in Regime III, the RDP is the oxygen-transport limited rate of debris formation. Figure 6b

shows the operative rate, this being the rate of the RDP at any point (i.e. the lowest of the three lines). From Figure 6b, the evolution of wear volume with the dissipated energy can be derived, this being simply the integral of the operative rate with energy; this is shown in Figure 6c where it can be seen that the rate ceases to increase linearly with the energy dissipated in the contact from the point that Archard-wear ceases to be the RDP.

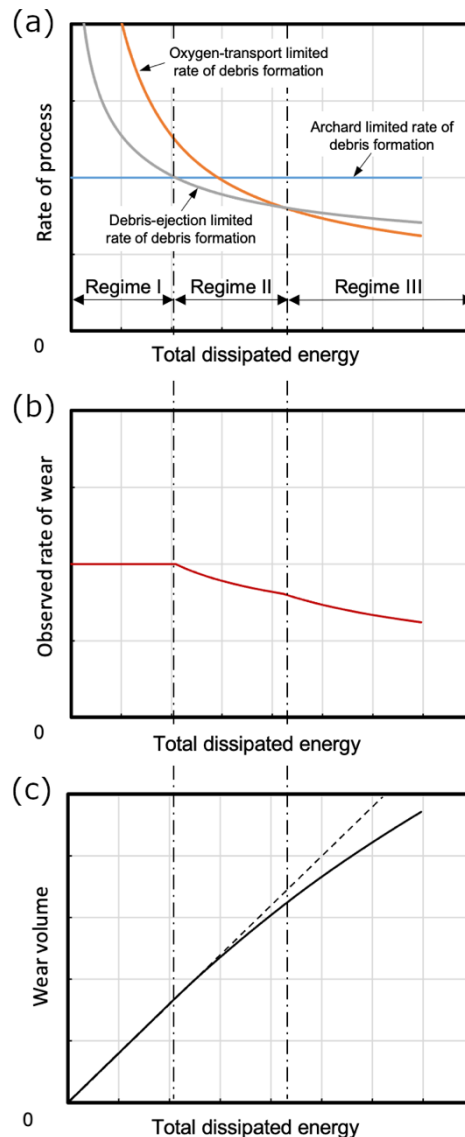


Figure 6. Schematic diagrams for fretting of a pair with a non-conforming contact geometry illustrating the variation with increasing dissipated energy of (a) rates of the three key processes; (b) the observed wear rate (i.e. the rate of the RDP); (c) total wear volume (where, for comparison, a line showing a wear volume which is directly proportional to the energy dissipated is also shown); the dashed lines across the three graphs indicate points of transition between the RDPs.

In later sections of the paper, the derivation of equations which may be used to describe these three rates are presented in detail, although it is recognised that the specific equations suggested are initial proposals, and each is likely to require significant further work to refine them. Despite this, it is argued that the key purpose of this paper remains valid, this simply

being to present and outline the concept of the three key processes within fretting and the concept of the RDP.

Once the three equations are in place, the operative wear rate at any point in a test can be derived (this being the lowest of the three), and from this a wear volume can be calculated. Using the equations derived for the rates of the three processes, the proposed dependence of each of these rates upon various parameters normally controlled in a fretting test (such as contact geometry, applied load, frequency etc) is outlined. To allow the concept of the RDP to be clearly outlined, the relevant equations will simply be presented in the following sections (with the physical basis behind the development of the equations for oxygen-transport limited rate of debris formation and the debris-ejection limited rate of debris formation being described in Appendices 1 and 2 respectively).

In order to allow equations to describe these three processes to be derived, a number of assumptions have been proposed with these assumptions being clearly identified in Appendices 1 and 2. It is recognised that whilst the assumptions made are reasonable, they have not been directly addressed in the literature, and thus they cannot be robustly justified at the current time. However, in seeking to present the concept of the RDP being key in understanding of behaviour in fretting, there is a need for those assumptions to be made (irrespective of how well justified they are). There is then of course a need for further experimental work to be conducted to examine the validity those assumptions, and to replace them within this framework if the evidence suggests that this is required. However, we argue that the suggestion that refinement of the assumptions will be required in future does not invalidate the general basis of the RDP approach being put forward here.

3.2 Rate of debris formation as described by the Archard wear equation (or similar) – Regime I

It has long been proposed that under certain situations (including fretting), the rate of wear in sliding (i.e. the rate of change of wear volume with energy dissipated in the contact) is a constant which depends only upon the two materials which make up the couple. This concept underlies the well-known formulation proposed by Archard [9] which (in cases where the coefficient of friction does not vary) is functionally equivalent to the energy-based wear rate (as first proposed by Fouvry and co-workers [6]) used here. This wear rate will be termed $\left(\frac{dV}{dE}\right)_{Arch}^{max}$ with the subscript “Arch” referring to “Archard”, and the superscript “max” indicating that this is the maximum possible rate of debris formation under Archard-type control. In accord with Archard’s proposal, it is assumed that this rate $\left(\frac{dV}{dE}\right)_{Arch}^{max}$ is a constant for a particular material pair.

3.3 Rate of debris formation controlled by oxygen transport into the contact - Regime II

The availability of oxygen right across the contact is required to ensure that oxide-based debris can be formed as part of the process of wear before it is expelled from the contact. The oxygen

concentration at the edge of the fretting contact will be that of the environment; however, within the contact, oxygen is consumed in the formation of oxide debris and therefore a concentration gradient in oxygen is formed across the contact which results in a diffusional flux of oxygen into the contact [36]. As a result of surface recession due to wear, the two bodies in Figure 3 approach each other with a rate $\left(\frac{dy}{dt}\right)$ which means that at each point on the surface, the sum of the recession (wear) rates of the two bodies at that point is equal to $\left(\frac{dy}{dt}\right)$. Accordingly, there needs to be sufficient oxygen transport into the contact from the environment to facilitate the formation of oxide-based debris at the same rate at all points within the contact. This also implies that oxygen must also be consumed in the formation of oxide-based debris at the same rate at all points within the contact and it is therefore clear that the oxygen concentration within the contact will be at its lowest on the contact centreline (i.e. at the point furthest from the edge of the contact).

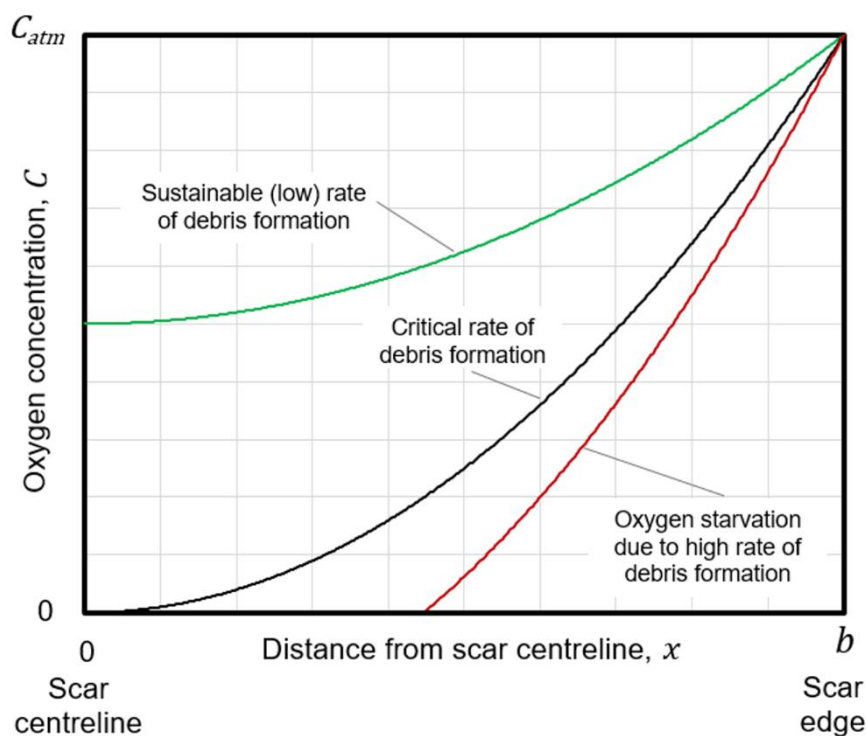


Figure 7 Illustration of variation of oxygen concentration across the contact for three different rates of debris formation. C_{atm} is the atmospheric oxygen concentration observed at the scar edge.

The driver for oxygen consumption is debris formation; in cases where the rate of oxygen transport into the contact is more than sufficient to meet the demands of debris formation, the oxygen concentration remains positive across the whole scar (illustrated by the green line in Figure 7). The time-based rate of consumption of oxygen (amount per unit time) will increase to meet any imposed demands for a higher rate of debris formation (driven for example by a higher fretting frequency or higher applied load) until a maximum rate is reached where the requirement that the rate of oxygen consumption (and therefore wear) is the same at every point in the scar can still be satisfied. The oxygen concentration across the scar under these conditions is illustrated by the black line in Figure 7 where it can be seen that the oxygen

concentration at the centre of the contact is zero; as derived in Appendix 1, an equation to describe this maximum rate is as follows:

$$\left(\frac{dV}{dE}\right)_{ot}^{max} = B \frac{C_{atm} D}{\delta^* \mu P f b^2} \quad \text{Equation 2}$$

The subscript “*ot*” refers to “oxygen transport” and the superscript “*max*” indicates that this is the maximum possible rate of debris formation under oxygen-transport control. *B* is a constant (with S.I. units of $\text{m}^6 \text{kg}^{-1}$), C_{atm} is the oxygen concentration in the atmosphere, *D* is the appropriate diffusion coefficient for transport of oxygen through the interface region, δ^* is the slip amplitude, μ is the coefficient of friction, *P* is the load applied across the contact, *f* is the fretting frequency, and *b* is the contact semi-width.

For completeness, it is noted that if a situation is considered where the rate of oxygen consumption across the scar would naturally be high due to a high rate of debris formation, then the oxygen profile across the scar would be as illustrated by the red line in Figure 7. In this case, the oxygen concentration would fall to zero before the scar centreline is reached (Figure 7); oxide-based wear debris could not be formed in the region of the scar where the oxygen concentration is zero and therefore (because of the need to maintain the same rate of wear at all points within the contact), the rate of surface recession (wear) across the whole contact would drop until the situation described by the black line in Figure 7 was re-established. The situation described by the red line is referred to as oxygen starvation and cannot be maintained in a continual, steady-state wear process (although it may exist in the initial-transient period before steady-state wear is established). It is noted that this proposal that sufficient oxygen is needed across the whole scar to maintain oxide formation is at odds with that espoused by Baydoun et al. [36,38] where it is suggested that the reduction in oxygen concentration as the distance from the edge of the fretting scar increases leads to a change from abrasive wear (where the oxygen concentration is high) to adhesive wear (where the oxygen concentration is low). However, we would argue that the framework that we have proposed is not in conflict with the experimental data presented by Baydoun et al. [36,38] where a lack of oxide wear debris is observed (by EDX analysis) towards the centre of the scars;

- (i) it is suggested that if this observation is made for a wear scar in the steady state (as opposed to the initial transient), this is consistent with the hypothesis that the oxide debris which is formed in these regions is transported away as fast as it forms which thus does not allow the build-up of a debris bed and thus results in metal-metal contact in this region;
- (ii) it is noted that the test durations in the work of Baydoun et al. [36,38] are quite short (20 000 cycles) and that for conforming contacts, these may still be in the initial transient period before steady-state wear is established. As such, the observation of a region which is devoid of oxide debris is consistent with the hypothesis that the debris layer has not yet been established in that region.

3.4 Rate of wear controlled by debris ejection from the contact - Regime III

In order that wear can continue (i.e. is not stifled in the way that it is when a glaze forms), oxide debris must leave the contact as fast as it is formed to prevent a build-up of debris (i.e. a continual thickening of the debris layer) in the contact. As derived in Appendix 2, the rate of wear controlled by the rate at which debris can be ejected from the contact (i.e. the rate with respect to energy dissipated in the contact) is given by:

$$\left(\frac{dV}{dE}\right)_{de}^{max} = \frac{G \beta}{\mu b} \quad \text{Equation 3}$$

The subscript “*de*” refers to “debris ejection” and the superscript “*max*” indicates that this is the maximum possible rate of debris formation under debris-ejection control. *G* is a constant which has S.I. units of m⁴ J⁻¹ and *β* is another constant which describes the fraction of the slip amplitude by which debris particles are displaced per cycle.

3.5 The observed wear rate

It was argued earlier that the observed rate of wear will be the lowest of rates of the three key processes which control wear. As such, in the absence of glaze formation, the wear rate observed in the system is given by the following:

$$\left(\frac{dV}{dE}\right)_{obs} = \min \left\{ \left(\frac{dV}{dE}\right)_{Arch}^{max}, \left(\frac{dV}{dE}\right)_{ot}^{max}, \left(\frac{dV}{dE}\right)_{de}^{max} \right\} \quad \text{Equation 4}$$

where the subscript “*obs*” indicates “observed”.

It is noted that whilst $\left(\frac{dV}{dE}\right)_{Arch}^{max}$ is a constant for a given material pairing, both $\left(\frac{dV}{dE}\right)_{ot}^{max}$ and $\left(\frac{dV}{dE}\right)_{de}^{max}$ are functions of the wear scar width, *b*. This is illustrated in Figure 5 (and in Figure 6a specifically for a non-conforming contact geometry), with its significance for fretting wear testing described as follows:

1. If the wear rate is controlled by the Archard wear equation throughout a test, the wear rate observed, $\left(\frac{dV}{dE}\right)_{obs}$, will be a constant. However, if the observed wear rate is controlled at any point during the test by either oxygen transport into the contact or by debris ejection from the contact, the wear rate will be less than that associated with the Archard equation.
2. With a non-conforming specimen pair geometry, the wear scar width, *b*, increases as the test proceeds. As such, both $\left(\frac{dV}{dE}\right)_{ot}^{max}$ and $\left(\frac{dV}{dE}\right)_{de}^{max}$ will become smaller as the test proceeds, and depending upon the conditions, may become the RDP during the test. As the wear scar width, *b*, increases, $\left(\frac{dV}{dE}\right)_{ot}^{max}$ (proportional to $1/b^2$) falls more rapidly

than $\left(\frac{dV}{dE}\right)_{de}^{max}$ which is proportional to $1/b$. This means that as b increases, the RDP may change from debris ejection to oxygen transport, but never vice versa.

3. With a non-conforming specimen pair geometry, if either $\left(\frac{dV}{dE}\right)_{ot}^{max}$ or $\left(\frac{dV}{dE}\right)_{de}^{max}$ become the RDP at any point during a test, the observed wear rate will continue to fall as the test proceeds. As such, the evolution of the wear volume with energy dissipated is dependent upon the history of the process, and therefore can only be determined by a time-marching method.

The structure of a suitable simple time-marching method to describe the evolution of wear volume with energy dissipated with non-conforming specimen pair geometries is illustrated in Figure 8.

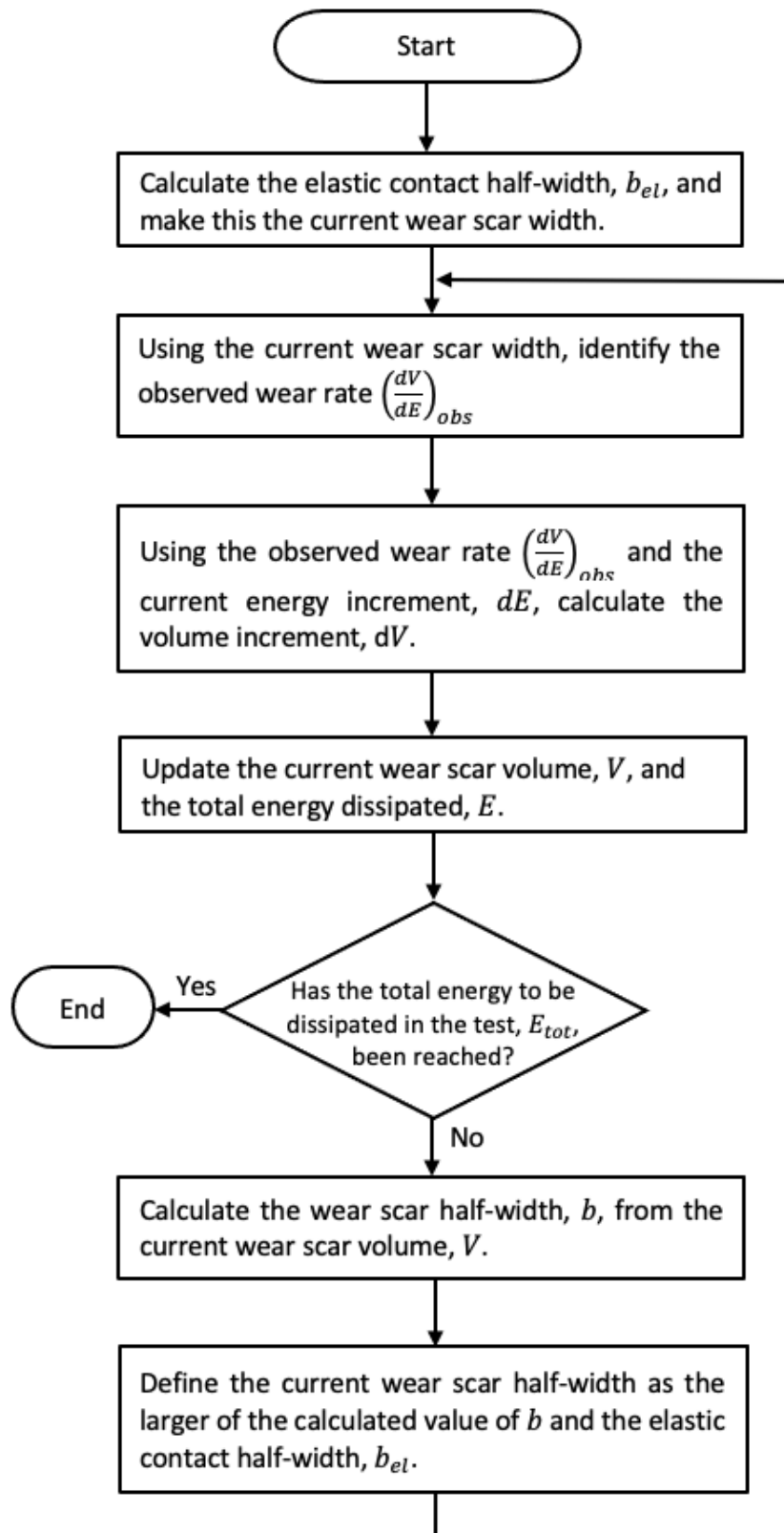


Figure 8 Basic process flow chart for the evolution of the wear scale volume as a function of energy dissipated in a contact between non-conforming specimen pairs.

The total energy dissipated in a test can be evaluated with the following equation:

$$E_{tot} = 4 \delta^* \mu P N \quad \text{Equation 5}$$

where E_{tot} is the total energy dissipated in a test of N cycles. In deployment of the time-marching model in this work, the energy increment for the initial steps has been set as $E_{tot} / 10^6$ until the accumulated energy reaches $E_{tot}/1000$; the energy increment was then increased to $E_{tot} / 10^5$ until the accumulated energy reaches $E_{tot}/100$, whereupon the energy increment is increased again to $E_{tot} / 10^4$ for the rest of the duration of the model.

The contact width at the beginning of the test is set as the elastic contact width, b_{el} . For the case considered here (that of a cylinder-on-flat contact with the two first bodies being both of the same material), the elastic contact width is given by the following standard equation:

$$b_{el} = \sqrt{8} \left(\frac{P R (1 - \nu^2)}{L \pi E_{Ym}} \right)^{1/2} \quad \text{Equation 6}$$

where E_{Ym} and ν are the Young's modulus and Poisson's ratio respectively of the two first bodies in the contact. If other non-conforming contact geometries are employed, then the appropriate equation simply needs to be employed in place of Equation 6.

The operative wear rate for the increment of energy dissipated, $\left(\frac{dV}{dE}\right)_{obs}$, is identified using the wear scar width at that point in the test, and using the appropriate energy increment, the total wear volume is incremented by that volume increment. Using the updated wear volume, the appropriate wear scar width is evaluated using an equation which relates the scar volume to the scar width. In the case of the non-conforming specimen pair that is being considered here (a cylinder-on-flat geometry), this is done by an interpolation method based upon Equation 1 which relates the scar volume and scar dimensions for a contact of this type. The operative wear scar width is then taken as the larger of that value (b) and the elastic contact width (b_{el}).

4 Tuning the model against experimental data

To summarise, the model is built upon four key hypotheses:

- the instantaneous rate of surface recession (wear), summed over the two specimens in the pair, must be the same at all positions within the wear scar (although it can vary temporally);
- wear occurs by the expulsion of oxide-based wear debris from the contact;
- oxide-based debris is formed at the same rate at all points within the contact which also requires that oxygen must also be consumed in the formation of that debris at the same rate at all points within the contact;
- debris expulsion per fretting cycle is inversely proportional to the contact size and is proportional to the slip amplitude.

We argue that the model is relevant for any metal for which these hypotheses are valid, although it is recognised that the model has been built around fretting between bodies made of steel and that further work is required to examine its validity for other systems (both metallic and non-metallic).

The model is based upon the three equations which describe various competing rates (as described in Equation 4); whilst each of the individual equations indicates the dependence of the particular process upon the fretting test parameters and conditions (including the instantaneous scar size, b), each equation also incorporates various constants, the values of which need to be defined for a particular system.

In defining the constants for the system under consideration, it is noted at this stage that this model is not currently in a form where it can be fully predictive. Instead, the model seeks to identify how the fretting test parameters and conditions (including the instantaneous scar size, b) influence the relative rates of the key physical processes, and thus influence which of these processes is rate determining in a given situation. As a result, the constants will also influence the prediction of the evolution of the wear volume under a given set of conditions.

To illustrate the application of this methodology, experiments related to the fretting wear of a high-strength steel (BS S132) against itself in a cylinder-on-flat specimen geometry conducted at the University of Nottingham are employed as the primary source of data against which the constants are tuned [9,11]. In our test facility, the applied far-field displacement amplitude (Δ^*) is controlled in a test, with the resulting slip amplitude in the contact itself (δ^*) being derived from fretting loops.

The slip amplitude can be related to the displacement amplitude as follows:

$$\delta^* = \Delta^* - \frac{\mu P}{S} \quad \text{Equation 7}$$

where P is the normal load across the fretting contact, μ is the coefficient of friction and S is the system stiffness (which incorporates the contact stiffness). In this work, a constant stiffness, S of $40 \text{ N } \mu\text{m}^{-1}$ has been employed which is in accord with experimental observations. It is recognised that the coefficient of friction, μ , is dependent upon the conditions of the test, and in some cases, varies within a test. However, the range over which μ varies is relatively small over a wide range of conditions. Given that currently we have no physical basis for the prediction of μ as a function of the test conditions, a constant value of 0.7 has been selected as being appropriate for the model predictions for the steel-steel pairs examined and is applied for all the test conditions.

The equations which describe the three processes which compete to control the observed rate of wear (as described in Sections 3.2 – 3.4) are presented in summary form in Table 1, with the values of the constants specified. In evaluating the constants, the time-marching approach was used which allowed any influence of the increasing scar size, b , to be accounted for; the details of how the constants were derived are outlined in the following sections (Sections 4.1 to 4.3).

Table 1 Summary of the competing rate equations (as described in Sections 3.2 – 3.4) and the evaluated and defined constants.

Physical process	Equation	Constants to be defined or evaluated	Value employed in the model
Archard wear (section 3.2)	$\left(\frac{dV}{dE}\right)_{Arch}^{max} = A$	A	$90 \times 10^{-15} \text{ m}^3 \text{ J}^{-1}$
Oxygen transport (section 3.3)	$\left(\frac{dV}{dE}\right)_{ot}^{max} = B \frac{C_{atm} D}{\delta^* \mu P f b^2}$	$(B \times D)$	$180 \times 10^{-21} \text{ m}^8 \text{ kg}_{O_2}^{-1} \text{ s}^{-1}$
		C_{atm}	$0.3 \text{ kg}_{O_2} \text{ m}^{-3}$
Debris ejection (section 3.4)	$\left(\frac{dV}{dE}\right)_{de}^{max} = \frac{G \beta}{\mu b}$	$(G \times \beta)$	$23.6 \times 10^{-18} \text{ m}^4 \text{ J}^{-1}$

4.1 The debris ejection constant ($G \times \beta$)

Previous work from the University of Nottingham [7] has addressed the dependency of the instantaneous wear rate on the width of the fretting scar for fretting in a cylinder-on-flat specimen pair arrangement. In that work, fretting tests with two different cylinder-on-flat geometries were employed (cylinders with radii of both 6 mm and 160 mm) over a range of test durations. The experimental results from that work are shown in Figure 9.

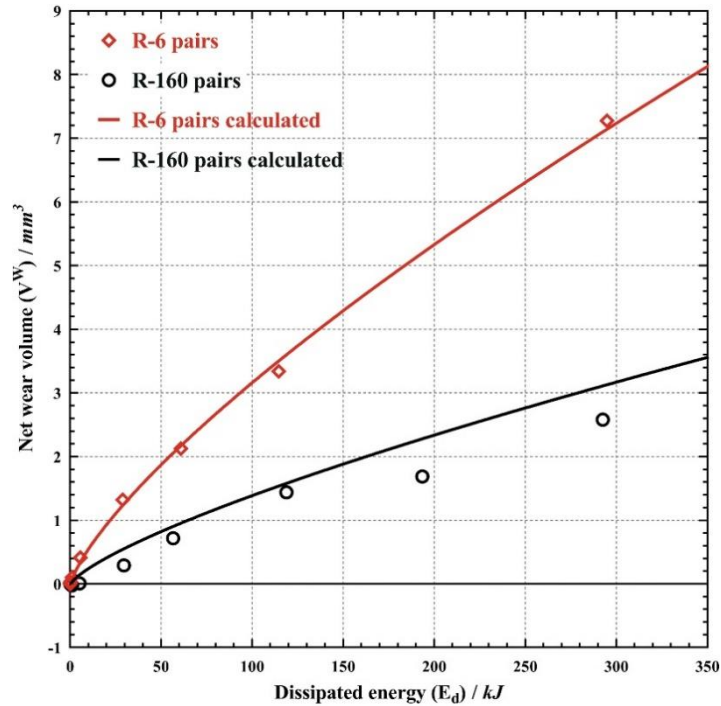


Figure 9 Experimental data from fretting tests with cylinder-on-flat geometry with cylinders with radii of 6 mm (R-6) and 160 mm (R-160). Alongside the data are calculated rates of wear for the two geometries based upon the assumption that the wear rate is directly proportional to the inverse of the wear scar width with the same constant of proportionality being employed for the two cases [9].

In the previous work [9], all fretting tests were conducted at 20 Hz and it can be assumed that under these conditions, the oxygen-access limited rate of debris formation, $\left(\frac{dV}{dE}\right)_{ot}^{max}$, was never rate determining (i.e. was never the smallest of the three rates). At the start of the test, the scar semi-width, b , is the elastic contact width, b_{el} (i.e. b is never zero) and so the debris-ejection limited rate of debris formation, $\left(\frac{dV}{dE}\right)_{de}^{max}$, is never infinite. In that previous work, the total test duration was large (5×10^6 cycles) and it was therefore assumed that the initial period where the Archard limited rate of debris formation would be operative (i.e. was the lowest of the three rates) was negligible. As such, it was assumed that the behaviour over the whole test was debris-ejection limited and therefore the behaviour could be described by:

$$\left(\frac{dV}{dE}\right)_{de}^{max} = \frac{\alpha}{b} \quad \text{Equation 8}$$

where α is a constant for the system being considered (i.e. is the same for different test geometries). Equation 8 is of the same form as Equation 3 (the rate of wear controlled by debris ejection from the contact as derived in this work); however, in the derivation in Appendix 2 of Equation 3 in Appendix 2, the roles of other parameters (e.g. applied load, slip amplitude, frequency) are also considered (these were not considered in work where Equation 8 was developed since they were not varied in the experimental programme upon which this was built [8]). The success of this general approach (and therefore a justification of the

assumptions made) is illustrated in Figure 9 where, with the value of α of $33.6 \times 10^{-18} \text{ m}^4 \text{ J}^{-1}$ derived in that work [9], the fit to the experimental data for the two different geometries is seen to be very satisfactory. In comparing Equation 3 and Equation 8, it can be seen that $G \beta = \alpha \mu$. Using the assumption (as discussed previously) that the coefficient of friction (μ) has a constant value of 0.7 allows the debris ejection constant ($G \times \beta$) to be evaluated as $23.6 \times 10^{-18} \text{ m}^4 \text{ J}^{-1}$ ($23.6 \times 10^{-3} \text{ mm}^4 \text{ kJ}^{-1}$).

4.2 The Archard wear constant (A)

As discussed in Section 4.1, in the work presented in Figure 9, the assumption was made that the initial period where the Archard rate of debris formation was rate-determining (i.e. was the lowest of the three rates) was negligible. This assumption becomes less valid for tests of smaller duration (i.e. where smaller values of energy are dissipated over the course of the test). In the test programme reported in Figure 9, tests had been conducted over a very wide range of durations (spanning the range 2000 cycles to 5×10^6 cycles) with a non-confirming fretting contact geometry (cylinder-on-flat); however, from this figure, the quality of the fit between the experimental data and the predictions are difficult to assess at the smallest test durations. In the small duration tests, the wear scar width is small and it is when the wear scar width is small that any influence of the Archard limited rate of debris formation would be most pronounced. As such, the data for the fretting tests with the same geometry as used in this work (i.e. for the 6 mm radius cylinder) are re-presented in Figure 10 on a log-log scale which enables the quality of the fit at the small test durations to be better assessed.

Using the time-marching methodology presented in this paper and making the assumption that oxygen-transport was never the RDP in these tests, the evolution of the wear volume with energy dissipated has been evaluated for various values of the Archard wear constant; five examples are presented in Figure 10 where comparisons can readily be made with the experimental data across the range. It can be seen that at the higher values of energy dissipated, the fit with experimental data is good irrespective of the value of the Archard wear constant selected (since here, the wear volume is dominated by the long period for which debris-ejection has been the RDP); however, at the smaller values of energy dissipated (where the effect of the Archard wear constant is most pronounced), it can be seen from Figure 10 that the data fit best with the model predictions with values of the Archard wear constant between $0.08 \text{ mm}^3 \text{ kJ}^{-1}$ and $0.1 \text{ mm}^3 \text{ kJ}^{-1}$. As such, it is proposed that a value of the Archard wear constant of $0.09 \text{ mm}^3 \text{ kJ}^{-1}$ ($90 \times 10^{-15} \text{ m}^3 \text{ J}^{-1}$) will provide an appropriate fit to these data, and this value will be employed for the remainder of the analysis as a constant for this material system.

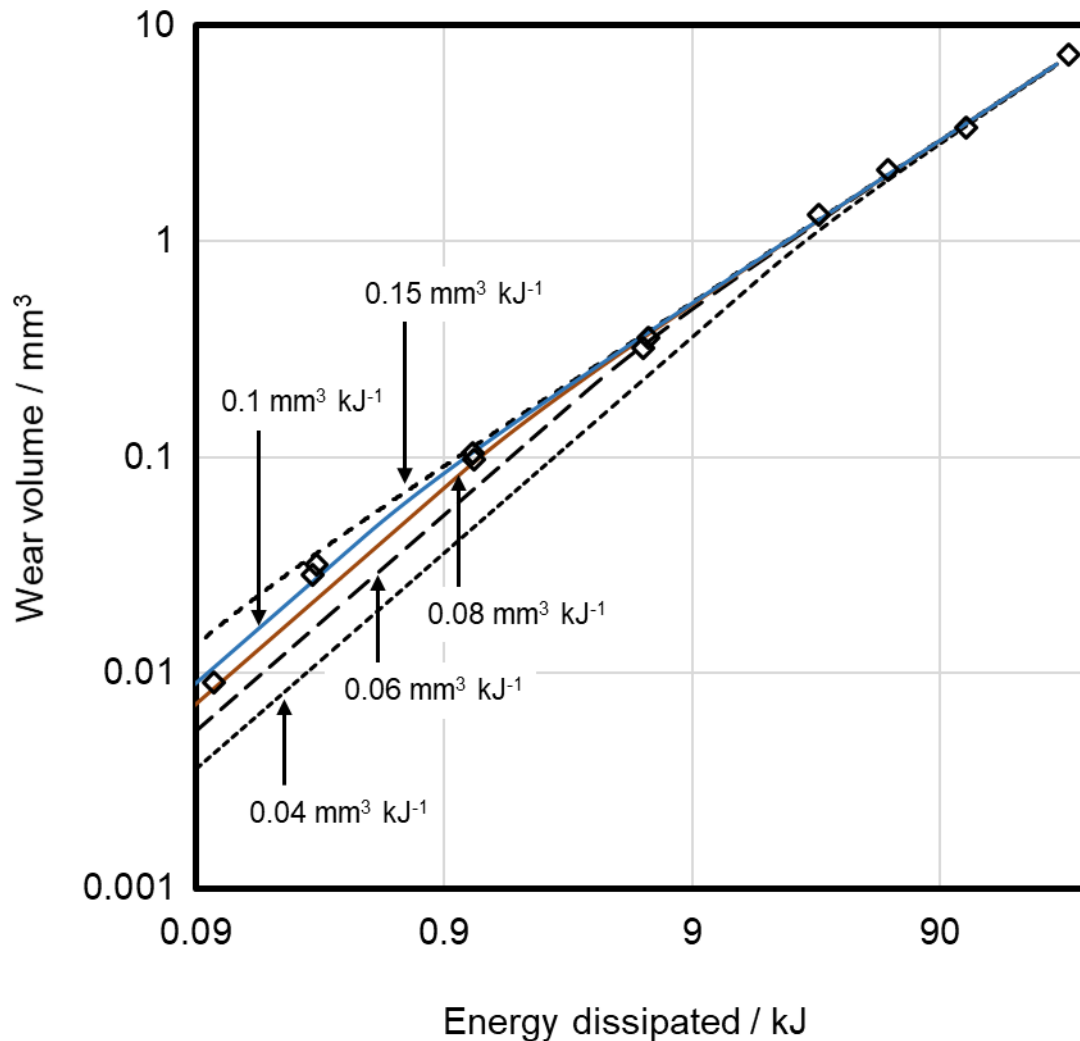


Figure 10 The data from Figure 9 for the R-6 pair presented on a log-log scale along with the predicted relationship between wear volume and energy dissipated using the time-marching technique with a range of values of the Archard wear constant as indicated.

4.3 The oxygen transport constant ($B \times D$)

Oxygen transport into the contact for the formation of oxide-based debris will become the RDP when the relevant line (the orange line) in a figure of the type illustrated in Figure 6a becomes the lowest of the three rates. The form of the equation for $\left(\frac{dV}{dE}\right)_{ot}^{max}$ (shown in Equation 2) indicates that low values are favoured by fretting with high values of frequency, applied load and / or slip amplitude. It is noted as an aside that these can perhaps more usefully be considered together and that (all other things being equal) the rate $\left(\frac{dV}{dE}\right)_{ot}^{max}$ is inversely proportional to the frictional power dissipation in the contact in accord with the work of Fouvry et al. [27]. Recent work [11] by the current authors examined fretting of the same steel under a range of displacement amplitudes and fretting frequencies for tests of duration of 1×10^6 cycles, again using the non-conforming cylinder-on-flat specimen pair geometry. Wear

volumes as a function of energy dissipated from this work are shown in Figure 11 where it is seen that the wear volumes as a function of energy dissipated are very similar for tests conducted at 20 Hz and 100 Hz but are significantly different for tests conducted at 200 Hz. The fact that at 20 Hz and 100 Hz, the behaviour is very similar (despite the changes in $\left(\frac{dV}{dE}\right)_{ot}^{max}$ associated with differences in the displacement amplitude and fretting frequency) indicates that under these conditions, $\left(\frac{dV}{dE}\right)_{ot}^{max}$ has not been rate determining for the bulk of the exposure to the fretting conditions.

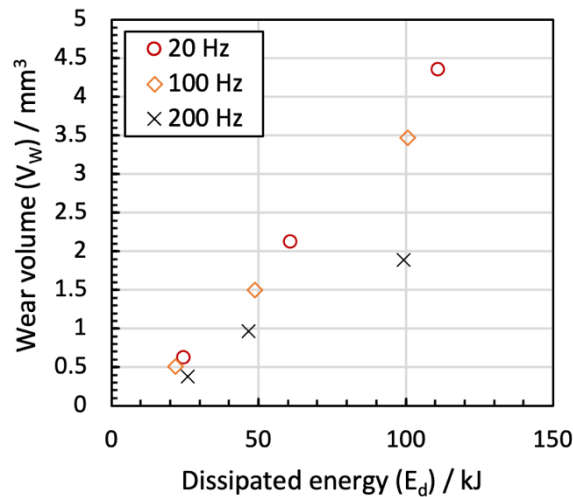


Figure 11 Wear volume after 10^6 fretting cycles as a function of dissipated energy for the three fretting frequencies examined as indicated; the three values of dissipated energy for each fretting frequency relate to the three displacement amplitudes employed in the tests (namely 25 μm , 50 μm and 100 μm) [11].

Moreover, an observation was made in this work [11] which related to the formation of an oxide bed in the contact under certain fretting conditions, but not under others. In accord with other work in the literature [27,35,39–41], extensive sub-surface deformation (normally termed the tribologically transformed structure (TTS)) was seen to develop when a substantial oxide debris layer was not present on the wearing surfaces to limit contact between the metallic first-bodies. Cross-sections though the wear scars from this previous work are reproduced (with annotations) in Figure 12; in the four cases indicated, significant subsurface damage was observed. With reference to the schematic diagram in Figure 6a, it is argued that when oxygen transport is not the RDP (i.e. the orange line is not the lowest of the three lines at any point during a test), then there will be a plentiful supply of oxygen into the contact to form debris, and as a result, first-body (metal-metal) contact which results in the formation of the TTS will not occur. Conversely, when oxygen transport is the RDP, the rate of debris formation (governed by oxygen transport into the contact) will be less than the maximum rate at which it could be removed from the contact. As such, a protective debris layer will not be formed within the contact, resulting in the development of a significant TTS. It is noted that metal-metal contact between two fretting surfaces will be observed in the initial transient period due to the absence of any oxide debris layer to separate the surfaces (irrespective of the fretting conditions) and that this will produce adhesive contact and a resultant TTS. This transient TTS

(along with the effects of any surface roughness) is normally eliminated by subsequent surface wear (as seen, for example, in the five the cross-sections presented in Figure 12 which are not annotated). The smallest depth of wear in those cases where no TTS was observed ($\Delta^* = 25 \mu\text{m}$, $f = 200 \text{ Hz}$) is around $10 \mu\text{m}$ [11] indicating that the initial transient TTS has a thickness less than this. Furthermore, it is noted that in the four cases where a TTS is observed in Figure 12, the maximum depth of wear is between $\sim 25 \mu\text{m}$ and $\sim 70 \mu\text{m}$, and thus it is argued that the TTS observed in these cases is not that associated with the initial transient period.

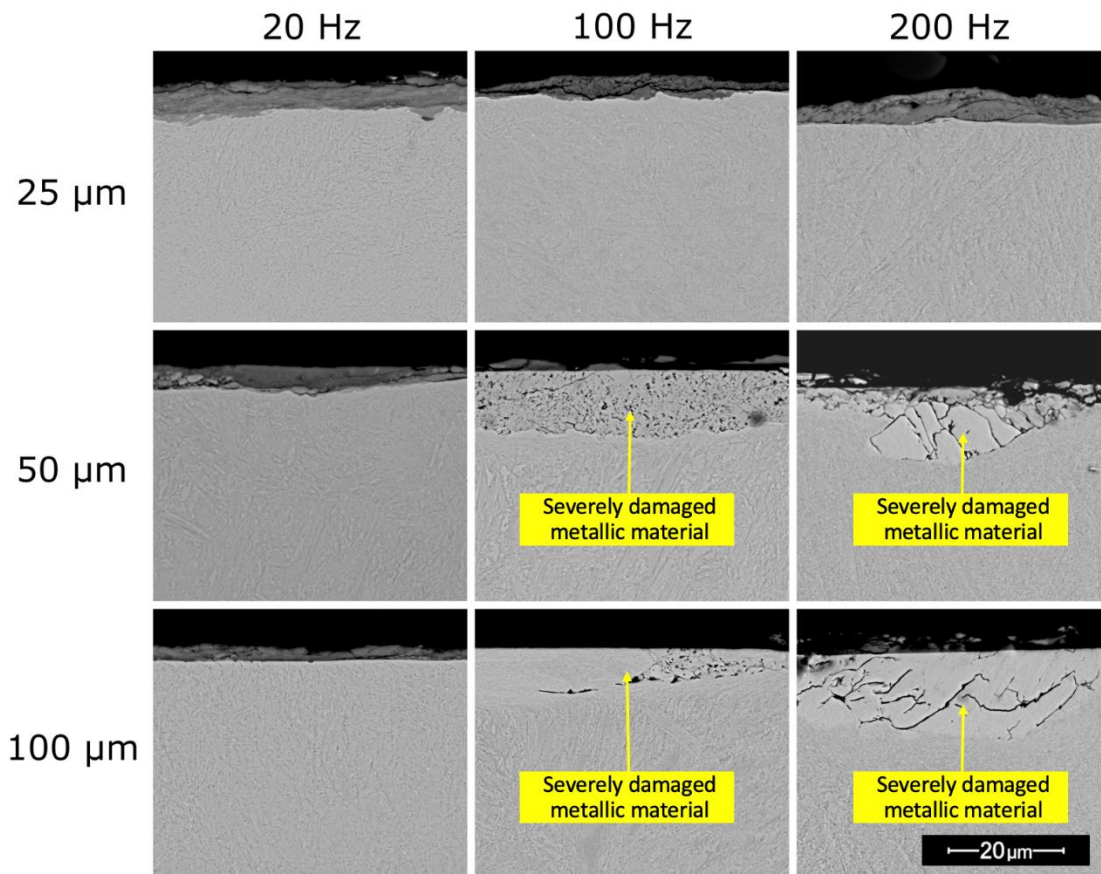


Figure 12 BSE SEM micrographs in sectional view of cylinder specimens after fretting for 10^6 cycles over the range of frequencies and applied displacement amplitudes examined, showing the development of significant levels of subsurface damage associated with increases in both parameters [11]. Fretting direction is left \leftrightarrow right in all cases.

The oxygen content in the atmosphere (C_{atm}) has a value of 0.3 kg m^{-3} (using a volume fraction of oxygen in air of 21% and a molar volume of $22.4 \times 10^{-3} \text{ m}^3$ at standard temperature and pressure). Ensuring that only the four cases exhibiting a TTS have oxygen transport as the RDP by the end of the test (i.e. the orange line is the lowest of the three lines by the end of the test in a plot of the type shown in Figure 6a) results in a requirement that $(B \times D) \leq 180 \times 10^{-21} \text{ m}^8 \text{ kg O}_2^{-1} \text{ s}^{-1}$ and this value will be employed for the remainder of the analysis as a constant for this system.

5 Holistic application of the model: the combined effect of frequency and slip amplitude in fretting

The effects of fretting frequency and displacement amplitude on wear mechanism can be assessed using the same set of experiments for which the model was tuned in the previous section, detailed in a previous paper by the current authors [11]. In this previous work, two broad classes of behaviour were defined that were observed to depend upon both frequency and displacement amplitude, namely (i) a regime associated with negligible subsurface damage despite significant levels of wear, termed oxygen-abundant fretting and (ii) a regime associated with the development of significant subsurface damage and reduced wear, termed oxygen-starved fretting. Oxygen-abundant fretting was observed at low displacement amplitudes (across the range of frequencies examined) and at low fretting frequencies (across the range of displacements examined), whilst oxygen-starved fretting is associated with increases in both parameters. It is noted here again that there will be a transient period of metal-metal contact at the beginning of all tests (even under oxygen-abundant conditions) due to the fretting of the two metallic bodies; in the case of oxygen-abundant conditions, this will persist only until a debris bed has formed which is able to separate the two first-bodies from each other. To illustrate the magnitude of this effect, a simple estimate of the debris layer thickness at the early stages of a test is made as follows;

- it is assumed that no debris leaves the contact area;
- it is assumed that all the metallic material worn from the specimens is converted to oxide in the form of Fe_2O_3 and that this has a volume 2.14 times greater than that of the metal from which it is formed (this being the Pilling-Bedworth ratio for this system);
- it is assumed that the debris forms a uniformly thick layer across the rectangular contact area (length L and width $2b$); the wear scar width $2b$ is a function of the amount of wear and is calculated in the manner indicated in Figure 8.

As an example, the initial transient evolution of debris thickness with energy dissipated is presented for the early stages of one of the cases considered in the experimental work which has underpinned this work, namely that of Kirk et al. [11]. The transient evolution of debris thickness is illustrated for two different cylinder radii in the cylinder-on-flat specimen pair geometry, these values being selected to align with the experimental work of Zhu et al. [9]. It can be seen that for the 6 mm radius cylinder-on-flat, the debris is predicted to build to a thickness of 5 μm (a nominal value chosen based upon the debris beds illustrated in Figure 12) after just 100 J of energy dissipation (~ 2000 fretting cycles) whereas the growth of a bed of equivalent thickness requires a duration of more than 1100 J (~ 20000 cycles) for the more conforming pair with the 160 mm cylinder.

A general conclusion here is that initial transient metal-metal contact will be observed (and that this will occur even in oxygen-abundant conditions), and that in considering RDPs in fretting, the test duration needs to be long enough that this initial transient can be safely ignored. Figure 13 indicates that the duration of the initial transient will be longer for contacts with larger areas (assuming that all other test parameters are the same), and therefore an

estimate of the duration of the initial transient metal-metal contact period should be made for research which is considering mechanisms of damage in fretting.

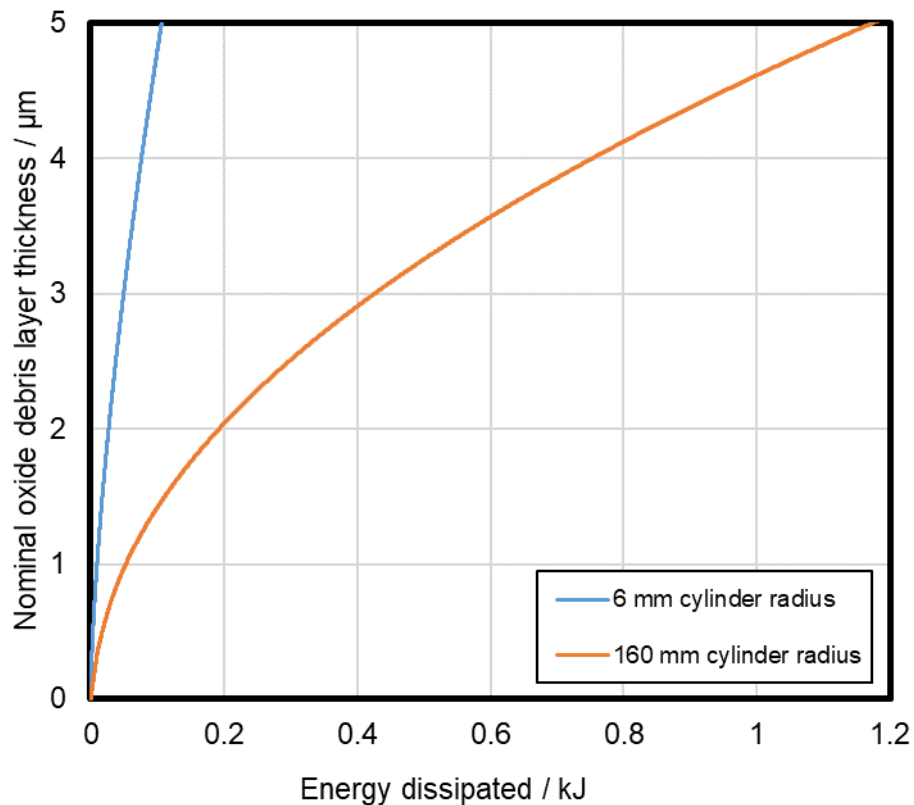


Figure 13 Prediction of development of oxide debris layer thickness in a contact for fretting of a cylinder-on-flat specimen pair under the conditions outlined in the work of Kirk et al. [11] for cylinders with radius of both 6 mm and 160 mm. The same applied load of 450 N was applied in each case with $\Delta^* = 50 \mu\text{m}$ and $f = 20 \text{ Hz}$.

Once the transient period has been addressed, the more general case can be considered. The evolution of RDPs predicted by the model over the range of frequencies and displacement amplitudes considered in the experimental work [11] are presented in Figure 14, in the same format as cross-sectional SEM images presented in Figure 12. In each case, the estimated frictional power dissipated is shown. It should be noted that (due to the same number of fretting cycles being deployed in all tests) the total energy dissipated during a test is dependent upon displacement amplitude, but not upon fretting frequency (since in the model, the coefficient of friction is assumed to be constant), and as such the range of the horizontal axis of the graphs presented in Figure 14 is the same across each row, but increases down each column. To aid comparison between parts of the figure, the spacing between the vertical gridlines has been fixed at 10 kJ in all cases.

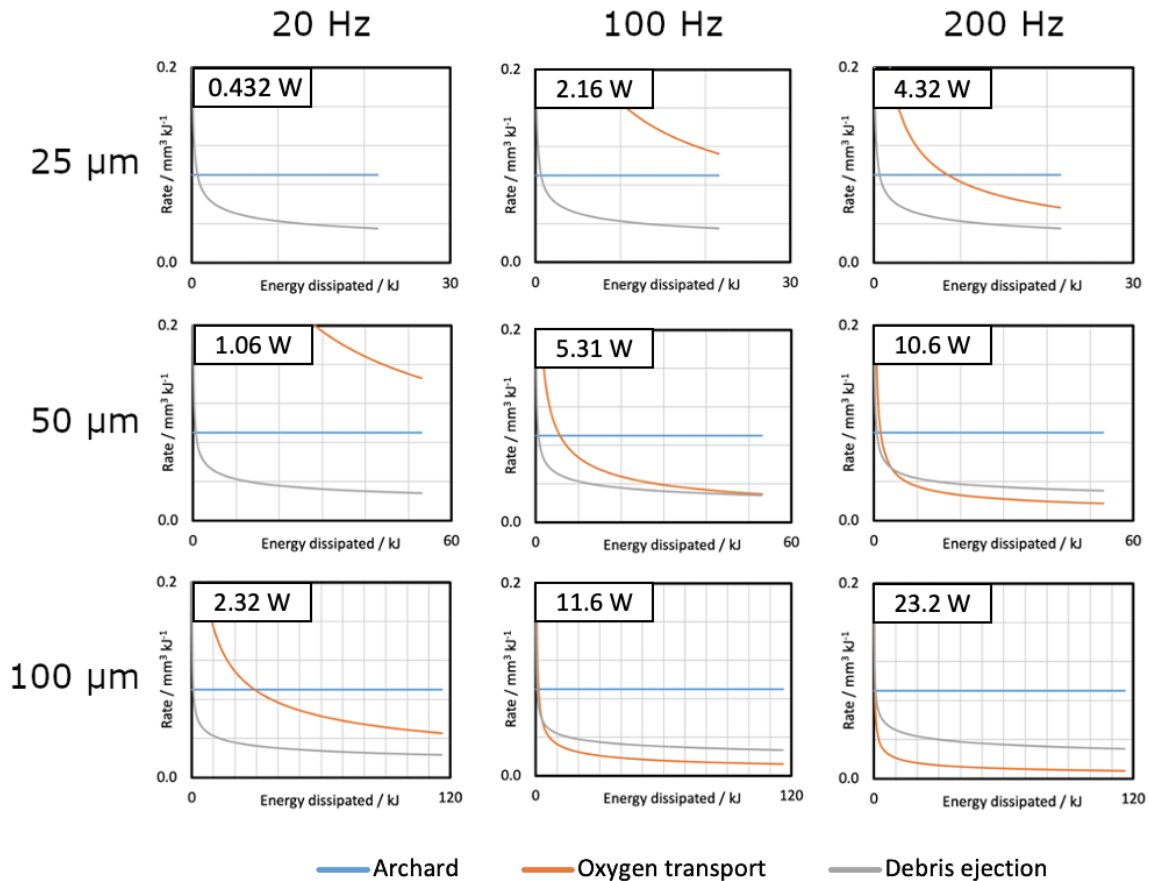


Figure 14. Evolution of RDPs (indicated by the process with the lowest rate at any point during a test) over the range of displacement amplitudes and frequencies studied experimentally [11]. Gridlines are spaced by 10 kJ in each of the graphs, highlighting the difference in total dissipated energy associated with changes in displacement amplitude ($P = 450 \text{ N}$; $N = 10^6$ cycles; $L = 10 \text{ mm}$). In each case, the frictional power dissipated (calculated using the assumptions made for the modelling work) is indicated.

At low displacement amplitude ($\Delta^* = 25 \mu\text{m}$) and low frequency ($f = 20 \text{ Hz}$), wear is predicted by the model to be limited by the rate of debris ejection from an early stage and to remain so throughout the duration of the test (Figure 14). With this displacement amplitude, the evolution of the rate of debris ejection with energy dissipated is the same for all three frequencies since oxygen-transport is never the RDP in these tests for any of the three frequencies examined. As such, the predicted wear volume at the end of these tests is the same for all three frequencies. As seen in Figure 14, increasing the frequency with any displacement amplitude results in the limiting rate of oxygen transport falling significantly; however, with $\Delta^* = 25 \mu\text{m}$, oxygen transport never becomes rate-determining at any point in a test for any of the frequencies, and as such the model predicts that in all of these cases there is sufficient oxygen transport into the contact to form oxide throughout the full width of the interface. These predictions align with the observations made in Figure 12 that no TTS is observed in any of the tests conducted with a displacement amplitude of $25 \mu\text{m}$ under these conditions.

Likewise, across the range of displacement amplitudes examined ($\Delta^* = 25 \mu\text{m}$ to $\Delta^* = 100 \mu\text{m}$), wear at low frequency ($f = 20 \text{ Hz}$) is predicted to be controlled by debris ejection for the

majority of the test duration. Here, there are different total energies dissipated in each case (since tests were run for a constant number of cycles) and thus the wear volumes are different. For the periods when debris ejection is the RDP, the wear rate falls monotonically with increasing energy dissipated meaning that the wear volume at the end of the three tests is not directly proportional to the energy dissipated. As previously, the limiting rate of oxygen ingress can be seen to fall significantly as displacement amplitude is increased (since this affects the frictional power dissipated and also – for tests with a fixed number of fretting cycles – the total energy dissipated), although oxygen transport does not become the RDP in any of the tests over this range of displacement amplitudes at this frequency and total duration. These predictions align with the observations made in Figure 12 that no TTS is observed in any of the tests conducted at 20 Hz under these conditions.

For the other four conditions considered (Figure 14), oxygen-transport becomes the RDP at some point in the test, and this results in each case in the formation of the distinct TTS associated with the failure to form an oxide bed in the contact (Figure 12). It is noted that with the test conditions of $\Delta^* = 50 \mu\text{m}$ and $f = 100 \text{ Hz}$, the rate of oxygen transport only becomes the RDP towards the very end of the test, with debris ejection being the RDP for the majority of the test duration; as such this is predicted to be a case in which the TTS is formed as a result of the conditions towards the end of the test, but where the wear volume at the end of the test is very similar to that of a similar test with a lower frequency since debris-ejection has been the RDP for the majority of the test.

In the other cases which exhibited significant TTS formation in Figure 12, it can be seen that oxygen-transport is the RDP from early stages of the test. For each of these three cases, the model predicts a reduced wear volume compared to the equivalent test conducted at 20 Hz (associated with the orange line being the lowest of the three and this limiting the observed rate of wear).

Care needs to be exercised in considering tests with different displacement amplitudes. It is recognised that an increase in displacement amplitude will result in a reduction in $\left(\frac{dV}{dE}\right)_{ot}^{max}$ (see Equation 2) due to its contribution to the frictional power dissipated in the contact; however, the increase in displacement amplitude also leads to an increase in total energy dissipated and therefore to a larger wear scar size (i.e. larger b) after a fixed number of cycles which again results in a lower value of $\left(\frac{dV}{dE}\right)_{ot}^{max}$ by the end of the test. It is this combined effect which makes the cases with similar frictional power dissipations to each other so different. A number of examples can be seen in Figure 14 where the power dissipated under two different sets of conditions is similar. In some comparisons (e.g. $\Delta^* = 25 \mu\text{m}$, $f = 100 \text{ Hz}$ and $\Delta^* = 100 \mu\text{m}$, $f = 20 \text{ Hz}$), the processes which are the RDP for the majority of the test and at the end of the test are the same. However, in the example of the comparison between $\Delta^* = 25 \mu\text{m}$, $f = 200 \text{ Hz}$ and $\Delta^* = 50 \mu\text{m}$, $f = 100 \text{ Hz}$, the debris ejection is the RDP for the majority of the test in each case, but due primarily to the extended duration (total energy dissipated) in the latter case, the RDP when the test completes is different (resulting in the very different types of damage being observed in the specimens following the tests – see Figure 12).

To clarify the impact of displacement amplitude on the relative rates of processes, Figure 15 shows the observed wear rate at any given point in a test (i.e. the rate of the RDP as shown in Figure 14) plotted on the same scale for all three displacement amplitudes at each frequency. It can be seen that at low frequency, the rate of the RDPs at each displacement amplitude overlay one another directly up to the respective dissipated energy of each condition. At higher fretting frequencies, the effect of displacement amplitude on observed wear rate becomes more pronounced; at a frequency of 100 Hz, a reduction in observed wear rate (over the shared range of dissipated energy) is only observed as displacement amplitude is increased above 50 μm , whilst at the highest fretting frequency ($f = 200$ Hz), a reduction in observed wear rate occurs with each increase in displacement amplitude above 25 μm .

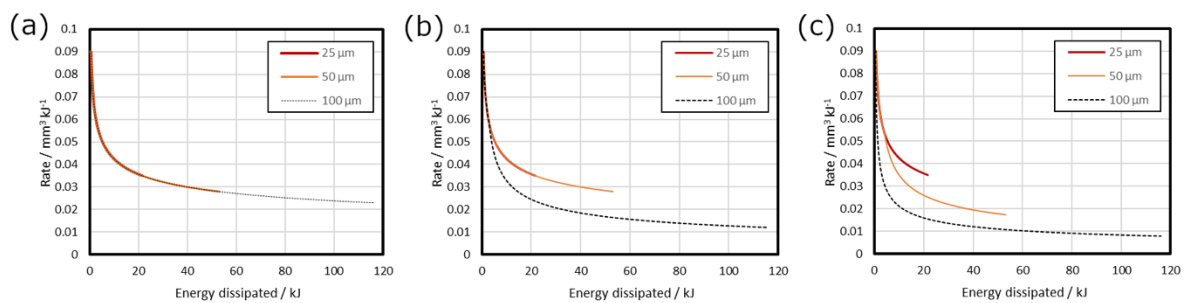


Figure 15. Observed wear rate (i.e. the rate of the RDP at a given dissipated energy) across the range of displacement amplitudes examined at a fretting frequency of (a) 20 Hz; (b) 100 Hz; (c) 200 Hz ($P = 450$ N; $N = 10^6$ cycles; $R = 6$ mm; $L = 10$ mm).

Figure 16 shows a comparison of the predicted and measured wear volumes for the experimental data presented in Figure 11. The correlation between the experimental data and model predictions are reasonable (but not strong); it is notable that at smaller displacement amplitude, the model predicts higher values than those observed experimentally, whilst at larger displacement amplitude, the model predicts smaller values than those observed experimentally. This indicates that some of the assumptions made in the development of the model regarding the dependencies of the three processes on the slip amplitude need detailed examination in future work; in particular, this indicates that there may be concerns over the validity of the assumption that the debris expulsion per fretting cycle is proportional to the slip amplitude (Appendix 2).

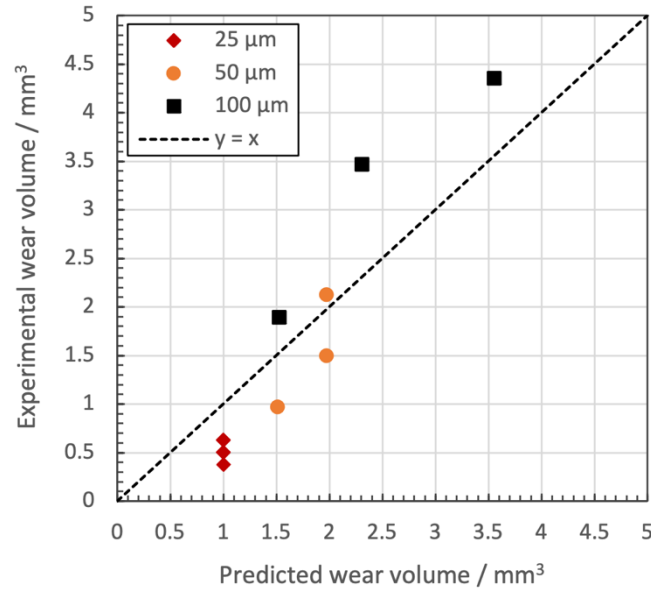


Figure 16 Comparison of predicted and measured wear volumes for the experimental data from the literature [11] (reproduced in Figure 11) with the line of equality marked.

In considering the comparison between the model predictions and experimental data (Figure 16), it should be noted that not only are there continual changes in the wear rate throughout each test due to the increasing size of the wear scar (b), but also there are changes in the RDP. An example of the predicted evolution of wear volume with energy dissipated is presented in Figure 17. All three tests represented here were modelled with 1×10^6 cycles and a fretting frequency of 100 Hz, but with different displacement amplitudes; the different displacement amplitudes led to different frictional power inputs and to different distances slid. In all tests, the instantaneous wear rate falls as the test proceeds, with this being associated with the increase in the scar width, b , as the amount of wear increases as a result of the use of a non-conforming contact geometry in this test programme.

It is also seen that the tests conducted with displacement amplitudes of 25 μm and 50 μm follow the same course (i.e. the wear volume at any given value of energy dissipated is the same in the two cases). However, this is not the case for the test with a displacement amplitude of 100 μm, indicating that different RDPs are operative. The contributions of wear under the different RDPs are presented in Figure 18 (the same data are presented in two formats to aid interpretation). In each case, the initial stage of the wear takes place with Archard wear as the RDP (blue section of the bar); as the scar increases in size as the energy dissipated is increased, a different process takes over as RDP, with this being debris ejection (grey section of the bar) in all but one case (that of the test conducted at 200 Hz with a displacement amplitude of 100 μm where oxygen transport directly takes over from Archard wear as the RDP as indicated by the orange section of the bar). In some of the cases where debris ejection was the second operative RDP, a transition to a third operative RDP (oxygen transport) occurs as the test proceeds, with this being indicated by the transition from the grey section of the bar to the orange section of the bar.

As a direct comparison with Figure 17, Figure 18a shows that at 100 Hz, the wear volumes with the fretting amplitudes of 25 μm and 50 μm are dominated by wear with debris ejection as the RDP, whereas with a 100 μm fretting amplitude, the majority of the wear volume is generated with oxygen transport as the operative RDP.

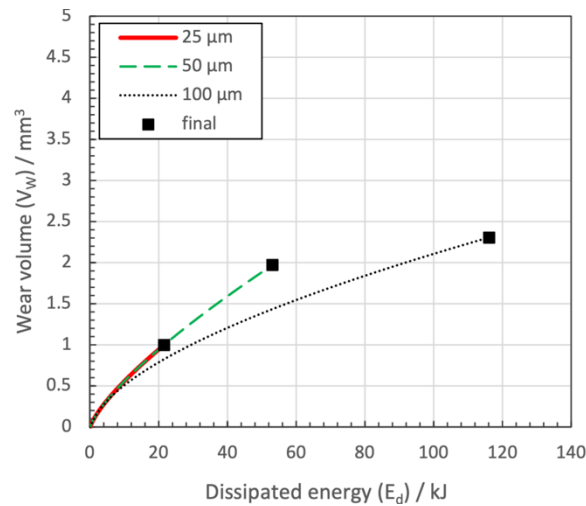


Figure 17 Evolution of predicted wear volume with increasing dissipated energy over a range of applied displacement amplitudes with fretting frequency of 100 Hz. Model conditions replicate those employed in generation of the experimental data presented in Figure 16.

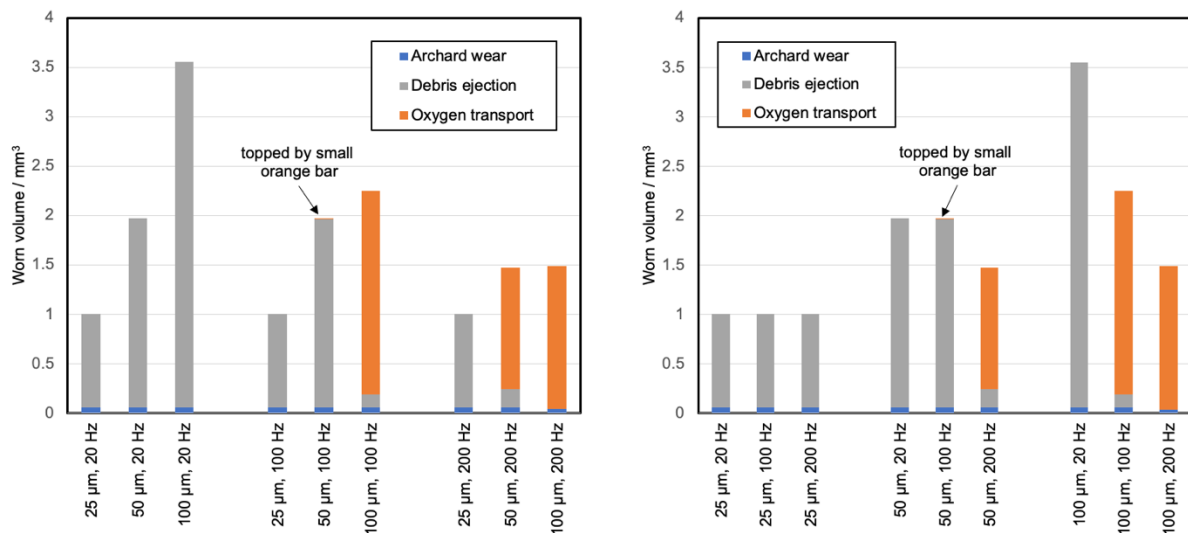


Figure 18 Predicted wear volumes for the different test conditions considered in the work behind the data presented in Figure 16 (displacement amplitude and fretting frequency were varied whilst number of cycles and applied load were kept constant). In each case, the wear volumes are sub-divided to show the fractions generated under the control of the three potential RDPs.

Figure 18a shows the predicted wear volumes (and the contributions of wear under the three RDPs to that total volume) separated by the frequency under which the test was conducted. At low frequency (20 Hz), debris ejection is the dominant RDP for all three displacement amplitudes and the wear volumes are observed to increase with displacement amplitude as expected (in broad accord with the relationship for a cylinder on flat contact that $V = A E^{0.75}$

[8]). However, at the two higher frequencies, it can be seen that the influence of oxygen transport being the RDP upon the final worn volume increases with increasing frequency, and results in a reduction in wear volume compared to that which might have been expected if debris ejection had remained the dominant RDP (i.e. the values of wear observed for the test conducted at 20 Hz). The same data are presented in a different format in Figure 18b to highlight the effect of frequency. Here, it can be seen that the frequency effect in fretting depends upon the conditions under which tests are conducted. With the cylinder-on-flat (i.e. non-conforming) experimental setup as described by Kirk at al. [11] with a fixed number of cycles and a fixed load, the model predicts that the wear volume will be independent of frequency at the lowest displacement amplitude of 25 μm , but will fall significantly with increasing frequency at the highest displacement amplitude (where at both 100 Hz and 200 Hz, oxygen transport is the RDP).

Figure 18 thus shows the importance of the use of a time-marching approach for non-conforming contact geometries in fretting, and shows that interpretation of the effects of various parameters on the progress of wear in fretting requires an understanding of which of the three processes identified is the dominant RDP.

6 The role of identification of the dominant RDP in a development of a coherent understanding of fretting wear

The equations which describe the three potential RDPs (as summarised in Table 1) indicate different dependencies of wear rate upon the various fretting parameters. This, coupled with an understanding of the contribution of wear under each of the three different RDPs to the total wear can give an indication of the expected influence of a particular test parameter on the overall wear volume observed in a test. These are summarised schematically in Table 2. Furthermore, Table 3 illustrates schematically how the magnitude of each parameter broadly influences which process is rate determining.

These two tables can be used together to develop an understanding of the influence of changes in test parameters on the observed rate of wear. As an example, Table 2 indicates that the applied load only affects the observed rate of wear, $\left(\frac{dV}{dE}\right)_{obs}$, when oxygen transport is the RDP, with Table 3 indicating that oxygen transport tends to become the RDP with high values of b , δ^* , μ , P and f and low values of C_{atm} .

Table 2 Predictions of the effect of change in various parameters on the observed wear rate depending upon the operative RDP. This information is a graphical representation of that contained in the equations presented in Table 1.




















Change in test parameter	Effect on parameter change on rate depending upon operative RDP		
	Archard wear	Oxygen transport	Debris ejection
b ↑			
C_{atm} ↑			
δ^* ↑			
μ ↑			
P ↑			
f ↑			

Table 3 Effect of changes in governing parameters on the operative RDP

Parameter	Tendency in operative RDP with increase in parameter		
			
b	Archard	Debris ejection	Oxygen transport
C_{atm}	Oxygen transport	Archard	Debris ejection
δ^*	Archard	Debris ejection	Oxygen transport
μ	Archard	Debris ejection	Oxygen transport
P	Archard	Debris ejection	Oxygen transport
f	Archard	Debris ejection	Oxygen transport

7 Discussion

The model presented in this paper is applicable to fretting with both conforming and non-conforming contact geometries, despite the fact that the data upon which the model has been tuned were derived from tests with non-conforming contact geometries. It is noted that the use of non-conforming geometries in fretting testing adds to the complexity of the situation as follows:

- If either debris ejection or oxygen transport is the RDP at any point in the test, then the instantaneous wear rate will decrease as the test proceeds. In these situations, the wear volume will not be proportional to the energy dissipated in the contact;
- The RDP that was operative upon the termination of a test will be the one reflected in any post-test sample characterisation; however, it should not be assumed that this was the RDP throughout the test. Moreover, tests where different amounts of wear take place due to the test duration alone (with all other parameters being the same) may exhibit different final RDPs (affected by the size of the wear scar) in any post-test sample characterization.

These complexities can be useful, but care is required in interpreting both the evolution of wear volume with energy dissipated and in considering the operative RDPs. Despite the experimental complexity of conducting tests with conforming contacts, it is recognised that there is a simplicity in the interpretation of the outputs given that the scar size does not change as wear proceeds. Perhaps more importantly, the outcome of this analysis points to the fact that in designing test programmes to simulate fretting conditions experienced in service, the physical dimensions of the contact (and the effect that this will have on oxygen transport and debris ejection) must not be ignored.

In assessing the capability of the model more generally to predict fretting behaviour there are two aspects to consider, namely (i) the evolution of wear volume with dissipated energy and (ii) the relative rates of key processes and which processes are rate-determining over a given set of conditions (i.e. the wear mechanism).

The relative rates of key processes (and hence wear mechanisms) predicted by the model exhibit good agreement with experimental observations over most of the conditions examined, although it is recognised that the difference between experimental and predicted wear volumes is generally not insignificant. The ability of the model to capture broad trends in wear volume and operative RDP over a broad range of parameters provide a promising indication of the predictive capability of the proposed framework, although the significant differences between observed and predicted wear volumes highlight that some of the assumptions involved in the model need to be fully evaluated and tested to identify the source of the discrepancies and hence improve the overall framework. As such, this discussion will address areas in which the model in its current form predicts changes in key processes, and identify areas where further work is needed to refine the approach to improve the accuracy of predictions and broaden the range of parameters over which it can be employed.

In Figure 16, it is observed that the model overestimates the wear volume at small displacement amplitudes (for which debris ejection is the RDP in the case considered here), and it is suggested that this overestimation results from the assumption (Appendix 2) that the rate of debris ejection is proportional to the slip amplitude, δ^* . It is recognised that the nature of this relationship is not well understood or justified and further work into the effect of displacement amplitude on debris ejection is required.

Another possible reason for discrepancies between predicted and observed wear volumes relates to the mechanism by which oxygen transport into the contact affects the formation of oxide debris; in the present work, restriction of oxygen transport to the interface only brings about changes in wear rate when oxygen transport becomes the RDP. As such, this mechanism does not account for any effects on contact oxygenation relating to the impact of fretting parameters on the thickness of oxide films formed between asperity interactions (as per the “oxidational wear” model of Quinn) [25,26,32,42,43]. It is noted that the mechanism of oxygen transport implemented in the model may be refined in future work to take into account effects of parameters such as applied load and displacement amplitude upon the transport of oxygen into the contacts (Appendix 1).

7.1 Considerations for future work

As mentioned previously, the physical framework outlined in this work is based upon a number of assumptions which have been made based on existing understanding of fretting mechanisms. However, some of the processes for which assumptions have been made (such as the relationship between the rate of debris ejection and the applied displacement amplitude, or the mechanism by which oxygen penetrates the contact) are not comprehensively understood; as such, detailed investigations into the effects of parameters such as displacement amplitude upon the key processes outlined in this chapter (namely oxygen ingress and debris ejection) are a critical area for further work in this area. The model has been deployed in a steel-steel fretting contact with a cylinder-on-flat geometry; there is a need to test the validity of the model for other metallic systems (including dissimilar pairs) and non-metallic systems, and for other test geometries (including conforming geometries).

The robustness of the model may also be improved by incorporating the effects of temperature on key processes, most notably the sintering of debris to form protective glaze layers, which have been found to significantly reduce wear rates. This could be achieved using a method similar to that developed by Dréano et al. [11,44], in which a “sintering parameter” is introduced to incorporate the effects of fretting parameters on local temperature, and thus adjust wear rate based on whether the sintering parameter is above or below a threshold value representing the critical temperature for glaze layer formation at a given set of conditions, the value of which may be based on experimental observations. Moreover, it is acknowledged that the values of proportionality constants employed in the present work (particularly the diffusion coefficient in the equation for oxygen transport) are expected to be temperature-dependent; in the present work, only fretting at room temperature is examined, and as such it is assumed that over the range of conditions examined, the effect of temperature on overall wear behaviour is small and therefore adequately represented in the tuning of the model to

experimental data (Section 4), although such an assumption may not be made when considering fretting at elevated temperatures.

Furthermore, the dependence of key processes upon contact size highlights the need for further understanding of how this dependence varies between different non-conforming contact geometries employed in fretting research, such as ball-on-flat and crossed-cylinder configurations. This involves investigating the geometrical relationship between contact width and wear volume in these different configurations, as the relationship employed in the present work is only relevant to the cylinder-on-flat case. In the same vein, care needs to be exercised in comparing fretting test data generated even in tests with conforming specimen geometries where the contact patch size differs.

Finally, it is recognised that the observation of a TTS in a contact following fretting can indicate that either the test was still in its initial transient period (before a stable debris bed thickness had developed) when the test was terminated, or that it was operating under oxygen-starved conditions when the test was terminated. Care needs to be taken to ensure that these two are distinguished in order to avoid drawing incorrect conclusions regarding the RDP based upon the microstructural characterisation; specifically, it is suggested that an assessment is made of the evolution of debris bed thickness under the assumptions made in producing Figure 13 and that tests are run for a duration where any observed debris-bed thicknesses are a small fraction of the nominal thickness, assuming that no debris leaves the contact.

8 Conclusions

It is proposed that wear rates can be modelled via the competition between three key processes which are required for fretting wear to proceed; it is the slowest of these which becomes the *rate-determining process* (RDP) and which governs the overall rate of wear. Equations are derived for rates of oxygen ingress and debris ejection which compete with the wear behaviour described by Archard to control overall wear rate; these equations are derived based on current understanding of the physics of fretting wear, but may be modified in future without disrupting the structure of this modelling approach based upon the RDP.

The competitive rate-determining method provides a method for modelling the role of debris in fretting wear, incorporating both the role of oxygen ingress to the interface in debris formation and the rate at which oxide is ejected from the contact, which are both critical in enabling wear to proceed. Whilst this can be readily deployed for fretting with conforming contacts, implementation of the model requires a simple time-marching method to be deployed in fretting of non-conforming contacts.

Future developments of the model may include modifying it to incorporate the effects of temperature (both environmental and local increase due to frictional power dissipation) on debris sintering, and hence the formation of glaze layers that have been reported to significantly reduce wear rates at high temperatures.

9 Acknowledgements

The authors would like to acknowledge Rolls-Royce plc for their support and funding of this research through the Transmissions University Technology Centre (UTC) at the University of Nottingham, UK.

10 References

- [1] M. Godet, The third-body approach: A mechanical view of wear, *Wear*. 100 (1984) 437–452. [https://doi.org/10.1016/0043-1648\(84\)90025-5](https://doi.org/10.1016/0043-1648(84)90025-5).
- [2] M. Godet, Third-bodies in tribology, *Wear*. 136 (1990) 29–45. [https://doi.org/10.1016/0043-1648\(90\)90070-Q](https://doi.org/10.1016/0043-1648(90)90070-Q).
- [3] Y. Berthier, L. Vincent, M. Godet, Velocity accommodation in fretting, *Wear*. 125 (1988) 25–38. [https://doi.org/10.1016/0043-1648\(88\)90191-3](https://doi.org/10.1016/0043-1648(88)90191-3).
- [4] Y. Berthier, L. Vincent, M. Godet, Velocity accommodation sites and modes in tribology, *Eur. J. Mech. A/Solids*. 11 (1992) 35–47.
- [5] C. Colombié, Y. Berthier, A. Floquet, M. Godet, Fretting: Load carrying capacity of wear debris, *J. Tribol.* 106 (1984) 192–200. <https://doi.org/10.1115/1.3260881>.
- [6] J.F. Archard, Contact and rubbing of flat surfaces, *J. Appl. Phys.* 24 (1953) 981–988. <https://doi.org/10.1063/1.1721448>.
- [7] S. Fouvry, T. Liskiewicz, P. Kapsa, S. Hannel, E. Sauger, An energy description of wear mechanisms and its applications to oscillating sliding contacts, *Wear*. 255 (2003) 287–298. [https://doi.org/10.1016/S0043-1648\(03\)00117-0](https://doi.org/10.1016/S0043-1648(03)00117-0).
- [8] T. Zhu, P.H. Shipway, Contact size and debris ejection in fretting: The inappropriate use of Archard-type analysis of wear data and the development of alternative wear equations for commonly employed non-conforming specimen pair geometries, *Wear*. 474–475 (2021). <https://doi.org/10.1016/j.wear.2021.203710>.
- [9] T. Zhu, P.H. Shipway, W. Sun, The dependence of wear rate on wear scar size in fretting; the role of debris (third body) expulsion from the contact, *Wear*. 440–441 (2019). <https://doi.org/10.1016/j.wear.2019.203081>.
- [10] P.H. Shipway, Time-dependence and exposure-dependence of material removal rates in fretting, *Wear*. (2021) 203826. <https://doi.org/10.1016/j.wear.2021.203826>.
- [11] A.M. Kirk, W. Sun, C.J. Bennett, P.H. Shipway, Interaction of displacement amplitude and frequency effects in fretting wear of a high strength steel: impact on debris bed formation and subsurface damage, *Wear*. 482–483 (2021). <https://doi.org/10.1016/j.wear.2021.203981>.
- [12] S.R. Pearson, P.H. Shipway, J.O. Abere, R.A.A. Hewitt, The effect of temperature on wear and friction of a high strength steel in fretting, *Wear*. 303 (2013) 622–631. <https://doi.org/10.1016/j.wear.2013.03.048>.
- [13] E.K. Hayes, P.H. Shipway, Effect of test conditions on the temperature at which a protective debris bed is formed in fretting of a high strength steel, *Wear*. 376–377 (2017)

- 1460–1466. <https://doi.org/10.1016/j.wear.2017.01.057>.
- [14] F.H. Stott, High-temperature sliding wear of metals, *Tribol. Int.* 35 (2002) 489–495.
- [15] J. Jiang, F.H. Stott, M.M. Stack, The role of triboparticulates in dry sliding wear, *Tribol. Int.* 31 (1998) 245–256. [https://doi.org/10.1016/S0301-679X\(98\)00027-9](https://doi.org/10.1016/S0301-679X(98)00027-9).
- [16] A. Viat, M.I. De Barros Bouchet, B. Vacher, T. Le Mogne, S. Fouvry, J.F. Henne, Nanocrystalline glaze layer in ceramic-metallic interface under fretting wear, *Surf. Coatings Technol.* 308 (2016) 307–315. <https://doi.org/10.1016/j.surfcoat.2016.07.100>.
- [17] A. Viat, G. Guillonneau, S. Fouvry, G. Kermouche, S. Sao Joao, J. Wehrs, J. Michler, J.-F. Henne, Brittle to ductile transition of tribomaterial in relation to wear response at high temperatures, *Wear.* 392–393 (2017) 60–68. <https://doi.org/10.1016/j.wear.2017.09.015>.
- [18] A. Dreano, S. Fouvry, G. Guillonneau, A combined friction energy and tribo-oxidation formulation to describe the high temperature fretting wear response of a cobalt-based alloy, *Wear.* 426–427 (2019) 712–724. <https://doi.org/10.1016/j.wear.2019.01.023>.
- [19] X. Jin, P.H. Shipway, W. Sun, The Role of Temperature and Frequency on Fretting Wear of a Like-on-Like Stainless Steel Contact, *Tribol. Lett.* 65 (2017) 77. <https://doi.org/10.1007/s11249-017-0858-0>.
- [20] A. Viat, A. Dreano, S. Fouvry, M.I. De Barros Bouchet, J.F. Henne, Fretting wear of pure cobalt chromium and nickel to identify the distinct roles of HS25 alloying elements in high temperature glaze layer formation, *Wear.* 376–377 (2017) 1043–1054. <https://doi.org/10.1016/j.wear.2017.01.049>.
- [21] F. Alkelae, S. Fouvry, Identification of parameters influencing the glaze layer formation and stability at high temperature for a Waspaloy/René125 contact under fretting wear conditions, *Wear.* 390–391 (2017) 41–48. <https://doi.org/10.1016/j.wear.2017.07.008>.
- [22] F.H. Stott, J. Glascott, G.C. Wood, Factors affecting the progressive development of wear-protective oxides on iron-base alloys during sliding at elevated temperatures, *Wear.* 97 (1984) 93–106. [https://doi.org/10.1016/0043-1648\(84\)90084-X](https://doi.org/10.1016/0043-1648(84)90084-X).
- [23] C. Mary, T. Le Mogne, B. Beaugiraud, B. Vacher, J.M. Martin, S. Fouvry, Tribochemistry of a Ti alloy under fretting in air: Evidence of titanium nitride formation, *Tribol. Lett.* 34 (2009) 211–222. <https://doi.org/10.1007/s11249-009-9426-6>.
- [24] C. Mary, S. Fouvry, J.M. Martin, B. Bonnet, Pressure and temperature effects on Fretting Wear damage of a Cu–Ni–In plasma coating versus Ti17 titanium alloy contact, *Wear.* 272 (2011) 18–37.
- [25] A. Iwabuchi, T. Kayaba, K. Kato, Effect of atmospheric pressure on friction and wear of 0.45% C steel in fretting, *Wear.* 91 (1983) 289–305. [https://doi.org/10.1016/0043-1648\(83\)90074-1](https://doi.org/10.1016/0043-1648(83)90074-1).
- [26] A. Iwabuchi, K. Kato, T. Kayaba, Fretting properties of SUS304 stainless steel in a vacuum environment, *Wear.* 110 (1986) 205–216. [https://doi.org/10.1016/0043-1648\(86\)90098-0](https://doi.org/10.1016/0043-1648(86)90098-0).
- [27] S. Fouvry, P. Arnaud, A. Mignot, P. Neubauer, Contact size, frequency and cyclic

- normal force effects on Ti–6Al–4V fretting wear processes: An approach combining friction power and contact oxygenation, *Tribol. Int.* 113 (2017) 460–473.
- [28] Y. Berthier, C. Colombié, L. Vincent, M. Godet, Fretting wear mechanisms and their effects on fretting fatigue, (1988).
- [29] I.M. Feng, B.G. Rightmire, An Experimental Study of Fretting, *Proc. Inst. Mech. Eng.* 170 (1956) 1055–1064. https://doi.org/10.1243/PIME_PROC_1956_170_089_02.
- [30] P.L. Hurricks, The mechanism of fretting - A review, *Wear.* 15 (1970) 389–409. [https://doi.org/10.1016/0043-1648\(70\)90235-8](https://doi.org/10.1016/0043-1648(70)90235-8).
- [31] D. Aldham, J. Warburton, R.E. Pendlebury, The unlubricated fretting wear of mild steel in air, *Wear.* 106 (1985) 177–201. [https://doi.org/10.1016/0043-1648\(85\)90109-7](https://doi.org/10.1016/0043-1648(85)90109-7).
- [32] I.M. Feng, H.H. Uhlig, Fretting corrosion of mild steel in air and in nitrogen, *J. Appl. Mech.* 21 (1954) 395–400.
- [33] B. van Peteghem, S. Fouvry, J. Petit, Effect of variable normal force and frequency on fretting wear response of Ti–6Al–4V contact, *Wear.* 271 (2011) 1535–1542. <https://doi.org/10.1016/j.wear.2011.01.060>.
- [34] A.R. Warmuth, P.H. Shipway, W. Sun, Fretting wear mapping: The influence of contact geometry and frequency on debris formation and ejection for a steel-on-steel pair, *Proc. R. Soc. A Math. Phys. Eng. Sci.* 471 (2015). <https://doi.org/10.1098/rspa.2014.0291>.
- [35] S. Baydoun, S. Fouvry, An experimental investigation of adhesive wear extension in fretting interface: Application of the contact oxygenation concept, *Tribol. Int.* 147 (2020) 106266. <https://doi.org/10.1016/J.TRIBOINT.2020.106266>.
- [36] S. Baydoun, P. Arnaud, S. Fouvry, Modelling adhesive wear extension in fretting interfaces: An advection-dispersion-reaction contact oxygenation approach, *Tribol. Int.* (2020) 106490. <https://doi.org/10.1016/j.triboint.2020.106490>.
- [37] S. Baydoun, S. Fouvry, S. Descartes, P. Arnaud, Fretting wear rate evolution of a flat-on-flat low alloyed steel contact: A weighted friction energy formulation, *Wear.* 426–427 (2019) 676–693. <https://doi.org/10.1016/j.wear.2018.12.022>.
- [38] S. Baydoun, P. Arnaud, S. Fouvry, Modeling contact oxygenation and adhesive wear extension in axisymmetric flat circular fretting interfaces, *Wear.* (2021) 203822. <https://doi.org/10.1016/j.wear.2021.203822>.
- [39] V. Nurmi, J. Hintikka, J. Juoksukangas, M. Honkanen, M. Vippola, A. Lehtovaara, A. Mäntylä, J. Vaara, T. Frondelius, The formation and characterization of fretting-induced degradation layers using quenched and tempered steel, *Tribol. Int.* 131 (2019) 258–267. <https://doi.org/10.1016/j.triboint.2018.09.012>.
- [40] J. Juoksukangas, V. Nurmi, J. Hintikka, M. Vippola, A. Lehtovaara, A. Mäntylä, J. Vaara, T. Frondelius, Characterization of cracks formed in large flat-on-flat fretting contact, *Int. J. Fatigue.* 124 (2019) 361–370. <https://doi.org/10.1016/j.ijfatigue.2019.03.004>.
- [41] J. Juoksukangas, V. Nurmi, J. Hintikka, M. Honkanen, M. Vippola, A. Lehtovaara, A. Mäntylä, J. Vaara, T. Frondelius, Cracks and degradation layers in large flat-on-flat fretting contact with steels and cast iron, *Tribol. Int.* 145 (2020) 106102.

<https://doi.org/10.1016/j.triboint.2019.106102>.

- [42] J. Jellison, R. Predmore, C.L. Staugaitis, Sliding friction of copper alloys in vacuum, *ASLE Trans.* 12 (1969) 171–182.
- [43] T. Akagak, D.A. Rigney, Sliding friction and wear of metals in vacuum, *Wear.* 149 (1991) 353–374.
- [44] A.M. Kirk, P.H. Shipway, W. Sun, C.J. Bennett, The effect of frequency on both the debris and the development of the tribologically transformed structure during fretting wear of a high strength steel, *Wear.* 426–427 (2019) 694–703. <https://doi.org/10.1016/j.wear.2018.12.035>.
- [45] A. Dréano, S. Fouvry, G. Guillonéau, A tribo-oxidation abrasive wear model to quantify the wear rate of a cobalt-based alloy subjected to fretting in low-to-medium temperature conditions, *Tribol. Int.* 125 (2018) 128–140. <https://doi.org/10.1016/j.triboint.2018.04.032>.
- [46] I. Iordanoff, Y. Berthier, S. Descartes, H. Heshmat, A review of recent approaches for modeling solid third bodies, *J. Tribol.* 124 (2002) 725–735. <https://doi.org/10.1115/1.1467632>.
- [47] N. Fillot, I. Iordanoff, Y. Berthier, Simulation of wear through mass balance in a dry contact, *J. Trib.* 127 (2005) 230–237.

Appendix 1 Derivation of rate equation related to oxygen transport

In this appendix, a proposal is made for a rate equation related to oxygen transport across a fretting contact. The general form of the equation is not derived from fitting of experimental data, but instead is based upon an understanding of the basic physics of the processes.

In fretting of metals, it is generally observed that the debris which leaves the contact is in the form of oxide which requires that oxygen flows into the contact to facilitate formation of that oxide at the interface. Under steady-state conditions, there will be no change in concentration of oxygen at a particular point with time; as illustrated in Figure 19, at a given element within the interface between the two fretting bodies, there is a balance between the oxygen flux in to the element, the rate of oxygen consumption in the debris formation process, and the oxygen flux out of the element.

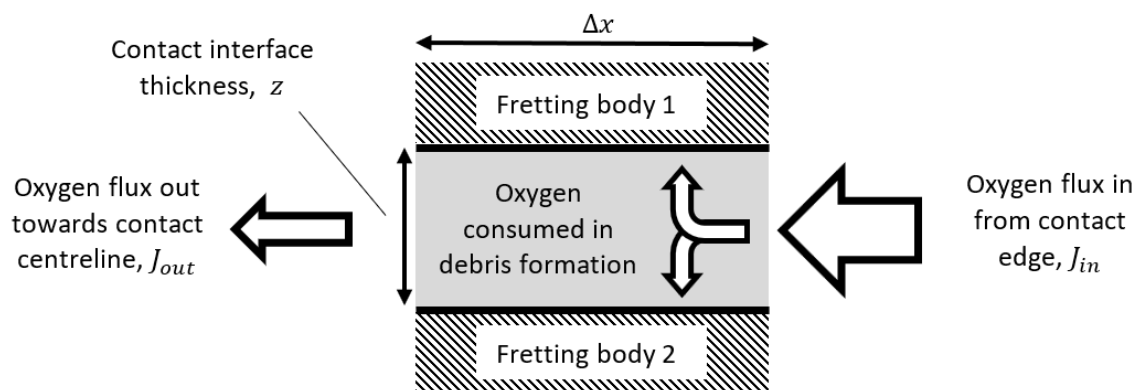


Figure 19 Illustration of oxygen flow and consumption in an element of the fretting contact interface. The interface has a line length of L , a thickness z and the element under consideration has a width Δx

An equation which describes this can be written as follows:

$$z L J_{in} = z L J_{out} + \dot{m} L \Delta x \quad \text{Equation A1.1}$$

where L is the length of the fretting contact and z is the contact thickness. J_{in} and J_{out} are the oxygen fluxes (with S.I. units of $\text{kg m}^{-2} \text{s}^{-1}$) in and out of the element respectively and \dot{m} is the consumption rate of oxygen (with S.I. units of $\text{kg m}^{-2} \text{s}^{-1}$) by reaction with the surface to make oxide at the rate required by the wear process, which (as was argued in section 3) needs to be the same across the whole contact.

As the width of the element, Δx , tends towards zero, Equation A1.1 can be rewritten as follows:

$$\frac{dJ}{dx} = -\frac{\dot{m}}{z} \quad \text{Equation A1.2}$$

In recent work considering oxygen transport into a fretting contact via a range of transport processes, it was argued that oxygen transport is mainly driven by diffusion [38]. Accordingly, we apply Fick's first law of general diffusion to oxygen transport through the contact interface, and write:

$$J = -D \frac{dC}{dx} \quad \text{Equation A1.3}$$

where C is the oxygen concentration (with S.I. units of kg m^{-3}) and D (with S.I. units of $\text{m}^2 \text{s}^{-1}$) is the appropriate diffusion coefficient for transport of oxygen through the interface zone.

The derivative of Equation A1.3 yields:

$$\frac{dJ}{dx} = -D \frac{d^2C}{dx^2} \quad \text{Equation A1.4}$$

Combining Equations A1.2 and A1.4 yields:

$$\frac{\dot{m}}{z} = D \frac{d^2C}{dx^2} \quad \text{Equation A1.5}$$

Now, in the case of a cylinder-on-flat fretting contact with oxygen transport into the contact from both contact edges, we have a symmetrical situation (see Figure 3) with the contact centreline as the line of symmetry. There can thus be no net flux of oxygen across the centreline of the contact, and therefore gradient in oxygen concentration at this point must be zero. With reference to Figure 7, we can therefore define boundary conditions as follows:

- a) when $x = b$ (i.e. at the scar edge), $C = C_{atm}$ where C_{atm} is the atmospheric concentration of oxygen;
- b) when $x = 0$ (i.e. on the scar centreline), $\frac{dC}{dx} = 0$

Integrating Equation A1.5 with these boundary conditions yields:

$$C = C_{atm} - \left(\frac{\dot{m}}{2zD} \right) (b^2 - x^2) \quad \text{Equation A1.6}$$

Oxygen starvation in the contact is defined as being when the required oxygen consumption rate, \dot{m} , cannot be sustained at all points across the scar. The lowest oxygen concentration anywhere in the system will be when $x = 0$; to avoid oxygen starvation therefore requires the oxygen concentration on the centreline to be greater than or equal to zero. Combining this constraint with Equation A1.6 yields the following requirement for oxygen starvation to be avoided in this situation:

$$C_{atm} > \left(\frac{\dot{m}}{2zD} \right) b^2 \quad \text{Equation A1.7}$$

Now, the consumption rate of oxygen required for debris formation, \dot{m} , will be directly proportional to the observed time-based rate of wear in the contact as follows:

$$\dot{m} = A \frac{dV}{dt} \quad \text{Equation A1.8}$$

where A is a constant with S.I. units of kg m^{-5} .

In a fretting test, the rate of energy dissipation is given as follows:

$$\frac{dE}{dt} = 4 \delta^* \mu P f \quad \text{Equation A1.9}$$

where δ^* is the displacement amplitude, μ is the coefficient of friction, P is the applied load and f is the fretting frequency.

Equation A1.9 can be employed in defining the time-based wear rate as follows:

$$\frac{dV}{dt} = \frac{dE}{dt} \frac{dV}{dE} = 4 \delta^* \mu P f \frac{dV}{dE} \quad \text{Equation A1.10}$$

Combining Equations A1.7, A1.8 and A1.10 yields an equation that defines when wear can proceed without oxygen starvation as follows:

$$C_{atm} > \left(\frac{2 A \delta^* \mu P f b^2}{z D} \right) \left(\frac{dV}{dE} \right)_{ot} \quad \text{Equation A1.11}$$

where $\left(\frac{dV}{dE} \right)_{ot}$ is the rate of wear controlled by oxygen transport. If it is assumed that z (the interface thickness) is a constant, then we can rewrite Equation A1.11 in terms of a maximum wear rate which can be sustained which is controlled by the oxygen transport into the contact, $\left(\frac{dV}{dE} \right)_{ot}^{max}$ as follows:

$$\left(\frac{dV}{dE} \right)_{ot}^{max} = B \frac{C_{atm} D}{\delta^* \mu P f b^2} \quad \text{Equation A1.12}$$

where B is a constant (with S.I. units of $\text{m}^6 \text{kg}^{-1}$) in which other constants are subsumed. The subscript “ ot ” refers to “oxygen transport” and the superscript “ max ” indicates that this is the maximum rate of at which oxide can be formed without oxygen starvation assuming that no other constraints operate.

By inspection, Equation A1.12 demonstrates that if wear is controlled by oxygen starvation, then the maximum rate of wear that can be sustained is proportional to both C_{atm} and D (itself a strong function of temperature and), and is inversely proportional to δ^* , μ , P , f and b^2 .

To allow a framework to be developed, it has been assumed that the diffusion coefficient D is independent of the nature of the debris layer (e.g. degree of compaction) through which

oxygen transport occurs and that the debris layer thickness (z) is a constant; however, it is recognised that validity of these assumptions will need to be explored in future work as this framework is refined.

Appendix 2 Derivation of rate equation related to debris ejection from the contact

In this appendix, a proposal is made for a rate equation related to debris ejection from the fretting contact, be that a conforming or non-conforming contact. The general form of the equation is not derived from fitting of experimental data, but instead is based upon and understanding of the basic physics of the processes. As argued previously, the rate at which surface recession (wear) proceeds at any time within a test is the same at any point within the fretting scar. If a non-conforming contact geometry is employed (such as the cylinder-on-flat configuration considered in detail in this paper), the wear scar increases in width as wear proceeds, and therefore new surface is continually brought into the wear process. As it is brought into the scar, new surface will experience an initial transient as damage develops, but then will continue to wear in steady state. It is notable that the debris thickness initially increases as a test commences, but it too reaches a steady state thickness; this indicates that in the steady state, wear debris is expelled from the contact at the same rate that it is created, and that there is therefore a steady flow of debris out of the contact from the position at which it was formed.

The flow of debris out of a fretting contact is complex, and a reasonable starting point might be that of rheology [18,45]; the flow will be facilitated by the oscillating motion between the two first bodies and we will assume that the total debris flow rate will be proportional to the slip amplitude, δ^* and also to the line length L (since the volume flow rate will simply scale with the length of the contact perpendicular to the direction of fretting). Treating the debris like a fluid allows us to assume that the debris flow rate from the contact is proportional to the applied pressure, p , (which in the case of the cylinder-on-flat contact is simply $(P/2bL)$); it is however, recognised, that flow of debris is promoted by the fretting motion, and that the primary flow is therefore in the direction of the fretting motion itself. The assumptions made here are an extension of those made in previous work where the flow rate of debris in a cylinder-on-flat contact (with constant values of applied load) was shown to be proportional to the wear scar width [46,47].

Proposals made in this section which require robust validation in future work are as follows:

$$(a) \quad \left(\frac{dV}{dN}\right) \propto \delta^*$$

$$(b) \quad \left(\frac{dV}{dN}\right) \propto p$$

Volumetric rates of oxide debris formation are proportional to rates of loss of metal from the first bodies with a constant of proportionality given by the Pilling-Bedworth ratio, R_{PB} , and in the steady state, the rate of debris expulsion from the contact must be equal to the rate of its formation. Together, these assumptions can be combined to yield an expression for the debris-ejection controlled wear rate as follows:

$$\left(\frac{dV}{dN}\right)_{de} = \frac{F L \beta \delta^*}{R_{PB}} \frac{P}{2 b L} \quad \text{Equation A2.1}$$

where $\left(\frac{dV}{dN}\right)_{de}$ is the rate of wear controlled by the rate of debris ejection from the contact, F is a constant (with S.I. units of $\text{m}^3 \text{N}^{-1}$), and β is the ratio of the net displacement of a debris particle per cycle and the slip amplitude. It is noted that β will depend upon the forces between individual particles within the debris bed.

We can define the frictional energy dissipated per cycle as follows:

$$\frac{dE}{dN} = 4 \delta^* \mu P \quad \text{Equation A2.2}$$

Equation A2.1 and Equation A2.2 can be combined to yield an expression for the maximum wear rate which can be sustained controlled by the rate of debris ejection from the contact, $\left(\frac{dV}{dE}\right)_{de}^{max}$ as follows:

$$\left(\frac{dV}{dE}\right)_{de}^{max} = \frac{G \beta}{\mu b} \quad \text{Equation A2.3}$$

where G (with S.I. units of $\text{m}^4 \text{J}^{-1}$) is a constant in which the other constants are subsumed.